Available online at www.sciencedirect.com

ScienceDirect

Advances in Space Research 77 (2026) 8269–8284

ADVANCES IN SPACE RESEARCH (a COSPAR publication)

www.elsevier.com/locate/asr

General properties of charged particle diffusion in heliosphere inferred from Forbush decreases

Stefano Della Torre [a,b,*], Giovanni Cavallotto [b,a], Giuseppe La Vacca [a,c,*], Massimo Gervasi [a,c]

[a] INFN Sez. Milano-Bicocca, Piazza della Scienza, 3, Milano 20126, Italy
[b] ICSC - Centro Nazionale di Ricerca in HPC, Big Data and Quantum Computing, Via Magnanelli, 2, Casalecchio di Reno, BO 40033, Italy
[c] Dipartimento di Fisica, Università degli Studi di Milano-Bicocca, Piazza della Scienza, 3, Milano 20126, Italy

Received 21 February 2025; received in revised form 9 April 2025; accepted 18 April 2025
Available online 23 April 2025

Abstract

Despite significant advancements in modeling solar modulation, the comprehension of the diffusion parameters remains challenging due to model parameter degeneracies and limited 3D *in situ* observations. Nevertheless, the study of Forbush decreases (FDs) still offers a natural probe for investigating particle transport properties. During FDs, coronal mass ejections and the associated magnetic disturbances propagating in the interplanetary medium enhance magnetic field turbulence, reducing diffusion of galactic cosmic rays (GCR). The result is a temporary reduction of GCR intensity, with recovery occurring over a few days. Previous studies linked FD observations to changes in diffusion parameters or turbulence levels, enabling insights into its rigidity dependence. In this work, we analyze five FDs observed by AMS-02 between 2011 and 2019 using a stochastic differential equation numerical code, based on the HELMOD-4/CUDA model, introducing localized changes to diffusion parameters in the inner heliosphere. Our results indicate that the rigidity dependence of the diffusion tensor remains consistent during both quiet and perturbed periods, suggesting that turbulences inducing FD do not fundamentally alter GCR propagation properties. These findings support the use of FDs to study particle transport in localized heliospheric environments, providing insights applicable to the broader heliosphere and improving diffusion modeling accuracy. These findings support the use of FDs to study particle transport in localized heliospheric environments, providing insights applicable to the broader heliosphere and improving diffusion modeling accuracy.

Keywords: Solar modulation; Forbush decrease; Heliosphere; EHC; SDE; Cosmic rays

1. Introduction

Propagation of galactic cosmic rays (GCR, also referred to as charged particles) in the interplanetary medium was successfully described by Parker (1965) as diffusion-dominated transport with adiabatic energy losses due to the expansion of the magnetized plasma (*i.e.,* Solar Wind, SW) permeating and defining the properties of the heliosphere (*i.e.,* the region where the solar wind is flowing out from the Sun) (see also, Gleeson and Axford, 1967; Gleeson and Axford, 1968; Jokipii and Parker, 1970; Jokipii, 1971; Fisk, 1971). The full description of the charged particle propagation in the heliosphere is usually referred to as *Parker transport equation* (PTE). This is a Fokker-Plank-like equation that includes other processes like convection, due to solar wind expansion, and drift of GCR gyro-radius guiding centers, due to large scale spatial gradients of the heliospheric magnetic field (HMF) (see, *e.g.,* Jokipii et al., 1977; Jokipii and Thomas, 1981; Jokipii and Levy, 1977; Potgieter and Ferreira, 2001; Engelbrecht et al., 2022, and reference there in). The

* Corresponding authors at: INFN Sez. Milano-Bicocca, Piazza della Scienza, 3, Milano 20126, Italy.
E-mail addresses: stefano.dellatorre@mib.infn.it (S. Della Torre), giuseppe.lavacca@unimib.it (G. La Vacca).

https://doi.org/10.1016/j.asr.2025.04.053
0273-1177/

combination of all these processes, produces the so-called *solar modulation* of GCR, *i.e.,* the observed variability of GCR intensity at energies $\lesssim 30$ GeV/n (see, *e.g.,* Gleeson and Urch, 1971; Caballero-Lopez and Moraal, 2004; Rankin et al., 2022a, and reference there in). Nowadays, the problem of the propagation of GCR in the heliosphere is well-known, but several aspects represent still open issues in heliophysics (see discussion in Engelbrecht et al., 2022). In particular, the attempt to model the diffusion term of PTE produced various theoretical models ranging from the quasi-linear theory (QLT) proposed by Jokipii (1966) to the non-linear guiding center (NLGC) theory of Matthaeus et al. (2003), and others (see, *e.g.,* Shalchi and Schlickeiser, 2004; Shalchi, 2010; Ruffolo et al., 2012; Qin and Zhang, 2014). In contrast, observations do not sample the heliospheric conditions exhaustively, with most of the observations at Earth orbit (*e.g.,* PAMELA-Adriani et al., 2013, SOHO-EPHIN-Kühl et al., 2017, AMS-02-Aguilar et al., 2018,...) and fewer observations in the deep-space (*e.g.,* Voyager 1–2-Stone et al., 1977, ...) and only one spacecraft probing the 3-D space of the heliosphere (*i.e.,* ULYSSES-Simpson et al., 1992). As disserted in Engelbrecht et al. (2022), there is a degeneracy in the parameters, which the model simplifications and assumptions cannot solve. This leads to a non-unique solution that can reproduce the data. Furthermore, it makes investigating the model parameters and their direct impact on global modulation phenomena not trivial. To further investigate this degeneration, additional sets of *in situ* measurements of GCR and plasma parameters are needed, as well as improving our capability to model the actual conditions of heliospheric plasma parameters at the location and the time in which those observations were taken (see discussion in Engelbrecht et al., 2022, and reference therein).

One of the reasons for the difficulty in breaking such degeneration is also related to the relatively sizable dimension of the heliosphere, whose boundary may be reached by HMF perturbations after several months (see discussion in, *e.g.,* Bobik et al., 2012; Tomassetti et al., 2017; Yang et al., 2025). Reducing the volume of the investigation to a relatively smaller region of the heliosphere (that in principle can be better probed) may allow one to better investigate the transport process. For instance, Engelbrecht et al. (2022) revised the so-called *Palmer consensus* (Palmer, 1982), *i.e.,* the range of acceptable values for electron and proton mean free paths in the inner heliosphere within a rigidity range of 0.0005-5GV, using Jovian electrons as test particles from a known source. This approach takes advantage of the fact that Jovian electrons transport to Earth orbit is dominated by parallel diffusion during good magnetic connections of Jupiter with Earth and by perpendicular diffusion during poor magnetic connections (see also Strauss et al., 2013; Vogt et al., 2020). The probing space is thus limited to a few astronomical units, *i.e.,* up to the radial distance of Jupiter. Nevertheless, the amount of reliable data for such a study is still limited and specific to low-energy electrons.

In this work, we explore the possibility of using the recovery phase of Forbush decreases (FD) to study the particle transport at intermediate rigidities (*i.e.,* > 1 GV) and in particular the diffusion coefficient of PTE, illustrated in detail in Section 2. FDs are a reduction of intensity in GCR spectra observed during interplanetary magnetic storms caused by powerful coronal mass ejection (CME), stream interaction regions (SIRs) and corotating interaction regions (CIRs) propagating in the interplanetary medium (Forbush, 1937; Forbush, 1954; Iucci et al., 1979; Cane, 2000; Cane and Richardson, 2003). The GCR intensity decrease is most probably produced by a reduced particle diffusion in the downstream turbulent region behind the front-shock of the event causing the storm (see, *e.g.,* Lockwood et al., 1991; Yu et al., 2010; Arunbabu et al., 2015), with a flux recovery occurring in a few days ($\sim$ 5–10 days in case of *sporadic* FD, see discussion in Wawrzynczak and Alania, 2008, and reference therein). Several works used the PTE to describe such a decrease in terms of a temporary localized diffusion reduction. In particular, we refer to Wawrzynczak and Alania (2008, 2010) and Luo et al. (2017, 2018). Wawrzynczak and Alania (2008, 2010) described several FDs with a three-dimensional non-stationary model; in their studies they found an inverse relationship between the rigidity spectrum index of the FD intensity at $\sim$10 GV, obtained combining observations from several neutron monitor stations at different locations, and the exponent of the power spectral density of the HMF in the frequency range $\sim 10^{-6} - 10^{-5}$ Hz.According to QLT, the diffusion term in the PTE should have a dependence in the form $K \propto R^{2-\nu}$, where ν is the IMF turbulence spectral index, thus, their study suggests that the rigidity dependence of $K_{||}$ is locally modified in the following area of a solar perturbation. Luo et al. (2017, 2018) included in their PTE numerical solution a *diffusion barrier model*, which is essentially a reduction of the absolute value of parallel/perpendicular diffusion parameter as well as the drift coefficient in the diffusion tensor of PTE in a specific region moving with the CME propagation. One may note that the first model implies that the exponent of the rigidity dependence of the diffusion term in the PTE changes due to the shock impact, which substantially means that the power spectral density of the turbulence in the HMF is modified through all the phases of the shock passage. The second approach, instead, supposes the very same diffusion model inside and outside the recovering region after the CME, with the level of turbulence described by the absolute value of the diffusion parameter. In this work, we aim to reproduce a selection of FD observed by AMS–02 (Aguilar et al., 2021; Wang et al., 2023) using an SDE numerical code derived by the HELMOD-4/CUDA code (Boschini et al., 2024) in which we modified the propagation in the innermost region (*i.e.,* $\lesssim 6$ AU). HELMOD-4/CUDA was designed to reproduce the long-term solar modulation. In the presented approach, we applied the most simple modification to HELMOD-4/

CUDA to prove the usability of this approach to study the particle transport during an FD period and, thus, infer some properties of the diffusion tensor.

2. Propagation numerical model

The transport of charged particles is described by the PTE, named after Eugene Parker who first proposed it in the 1960s (see, e.g. Parker, 1965; Boschini et al., 2019, and references therein):

$$\frac{\partial \mathrm{U}}{\partial t} = \frac{\partial}{\partial x_i}\left(K^S_{ij}\frac{\partial \mathrm{U}}{\partial x_j}\right) \tag{1}$$

$$+\frac{1}{3}\frac{\partial V_{\mathrm{sw},i}}{\partial x_i}\frac{\partial}{\partial T}(\alpha_{\mathrm{rel}} T\mathrm{U}) - \frac{\partial}{\partial x_i}[(V_{\mathrm{sw},i}+v_{d,i})\mathrm{U}],$$

where U is the number density of GCR particles per unit of kinetic energy T (GeV/nucleon), t is time, $V_{\mathrm{sw},i}$ is the solar wind (SW) velocity along the spatial coordinate x_i for $i=\{1,2,3\}$, K^S_{ij} is the symmetric part of the diffusion tensor, $v_{d,i}$ is the particle magnetic drift velocity (related to the antisymmetric part of the diffusion tensor), and $\alpha_{\mathrm{rel}} = \frac{T+2m_rc^2}{T+m_rc^2}$, with m_r the particle rest mass per nucleon in units of GeV/nucleon. In the form written in eq. (1), PTE displays the four physical processes involved in GCRs transport: diffusion, adiabatic energy loss, convection, and magnetic drift. These processes vary according to the intensity level and phase of solar activity, the intensity, and polarity of the solar magnetic field, and are rigidity- and charge-sign-dependent.

To evaluate the modulated GCR spectra, eq. (1) is usually solved numerically, given the GCR differential intensities at the boundary as the primary input, *i.e.,* outside the heliosphere, also known as the (very) local interstellar spectrum (LIS). Nowadays, it has become of common use in the scientific community to solve PTE employing the Monte Carlo integration of an equivalent set of stochastic differential equations (SDE, see, *e.g.,* Effenberger et al., 2012; Kopp et al., 2012; Zhao et al., 2014; Bobik et al., 2016; Boschini et al., 2019; Moloto et al., 2019; Vogt et al., 2020). This approach presents several advantages in terms of stability of the solution and modularity of the code, and allows expanding the model's functionality with relatively small changes in the code. For this work, we based our calculation on the HELMOD-4/CUDA (Boschini et al., 2024) code, a version of the HELMOD-4 model running on GPUs architecture for an increase in computation performances (see, e.g., Dunzlaff et al., 2015; Vogt et al., 2020; Solanik et al., 2021; Solanik et al., 2023).

The HELMOD-4 model is a Monte Carlo code, that solves the PTE using the SDE backward-in-time numerical technique. HELMOD-4 is a model that in the last years was specialized to (successfully) reproduce the long-term solar modulation (Bobik et al., 2012; Della Torre et al., 2012; Boschini et al., 2018a; Boschini et al., 2019; Bartocci et al., 2020; Rankin et al., 2022b), with an accuracy level comparable to the actual experimental uncertainties (*i.e.,* a few percent for AMS-02 time-integrated spectra). The code, used in combination with GALPROP (Boschini et al., 2017) has been used to infer the LIS for particles with the atomic number up to $Z=28$ (Boschini et al., 2018b; Boschini et al., 2018c; Boschini et al., 2020a; Boschini et al., 2020b) allowing to highlight fine structures in GCR observed spectra (Boschini et al., 2021; Boschini et al., 2022a; Boschini et al., 2022b). Finally, it was demonstrated that the model is also suitable for assessing the potential radiation risk in the space environment (see, *e.g.,* Boschini et al., 2022c; Liu et al., 2024).

The complete description of the model and its numerical implementation can be found in Boschini et al. (2024) and references therein. Here we recall the main aspects relevant to this work. Following the so-called quasi-linear theory (QLT) under the approximation of a weak turbulence, and the commonly accepted behavior for the diffusion tensor parallel to IMF ($K_{\parallel}$), in the model we implement the formulation described in Boschini et al. (2018a) and consistent with those presented in Section 3.1.1. in Burger and Hattingh (1998):

$$K_{\parallel} = \frac{\beta}{3}K_0\left(\frac{P}{1\mathrm{GV}}+g_{\mathrm{low}}\right)\left(R_c+\frac{R}{1\mathrm{AU}}\right), \tag{2}$$

where K_0 is the diffusion parameter evaluated using the procedure described in Bobik et al. (2012) and updated in Boschini et al. (2018a) and Boschini et al. (2024), β is the particle speed in units of the speed of light, $P=qc/|Z|e$ is the particle rigidity in GV, R is the heliocentric distance from the Sun in AU, and, finally, g_{low} and R_c are dimensionless parameters tuned to describe radial GCR intensity gradients in the inner heliosphere (see also discussions in Boschini et al., 2019, and references therein). This formulation has the advantage of keeping the number of free parameters as small as possible. Nevertheless, as showed in Tomassetti et al. (2025), even a more general $K_{\parallel}$ functional, such as a double power law rigidity dependence (see, *e.g.,* Aslam et al., 2021), is equivalent to a linear dependency with respect rigidity, after the model tuning on experimental data. To allow the model to reproduce low energy latitudinal gradients as described in Section 3.2 of Boschini et al. (2018c) and Section 5.4 in Boschini et al. (2018a) we refined the Parker magnetic field adding a polar correction (described in Section 2.4 of Boschini et al., 2018a) that increases the intensity of magnetic field through a small, but not negligible, latitudinal component (see discussion in Jokipii and Kota, 1989). The perpendicular diffusion coefficient is assumed to be directly proportional to $K_{\parallel}$, with the ratio of $K_{\perp,i}/K_{\parallel}$ being approximately 0.065 for protons and 0.050 for electrons, for both radial and latitudinal coordinates of the diffusion tensor (Boschini et al., 2018a). As reported in Boschini et al. (2019), the slight difference between those values might be related to the mass differences between nuclei (including protons) and leptons (i.e., electrons and positrons). As discussed in Bobik et al. (2012), we have used $K_{\perp,\theta}$ enhanced by a factor 2 in

Table 1
FDs selected from Table 3 in Wang et al. (2023).

FD	Solar Activity	FD start	Min. Flux Day	MAR [GV]	Ampl [%]	Simulated days
006	ICME	2011–08-06	2011–08-06	16.6	13.6 ± 0.4	13
010	ICME	2011–10-25	2011–10-25	48.5	10.3 ± 0.5	12
017	ICME	2012–03-08	2012–03-09	33.5	35.1 ± 0.5	28
058	CIR	2014–02-28	2014–03-01	33.5	10.0 ± 0.5	19
121	ICME	2017–09-08	2017–09-08	22.8	17.7 ± 0.3	11

the polar regions to accurately model the amplitude and rigidity dependence of the latitudinal gradients of GCR differential intensities for protons. This correction is an implicit way of reducing drift effects in polar regions (see Potgieter, 2013; Vos and Potgieter, 2016; Boschini et al., 2018a, and references therein). The drift model used in HELMOD-4 was based on the model described in Potgieter and Moraal, 1985, which was modified to include the polar correction of the magnetic field, and the suppression factor at rigidities below 1 GV during high-activity periods and an additional effective drift suppression tailored for rigidities above 10 GV around solar activity minimum, as described in Boschini et al. (2024) and references therein. To account for the time needed for an HMF perturbation to propagate up to the external boundary, the simulated heliosphere is divided into 15 + 1 radially equally spaced regions, the first 15 regions are inside the termination shock boundary, while the additional region is the heliosheath. The i-th region crossed by CR particles is characterized by a set of heliospheric plasma parameters evaluated at the Carrington rotation located in the past at a time corresponding to the time needed by SW for reaching it (see discussion in Bobik et al., 2012; Boschini et al., 2019). The diffusion description and the shape of the heliosphere from the HELMOD-4 version used in this work are computed in a 3D space. In particular, this study involves only modifying the intensity of the diffusion term K_0. It is important to remark that in principle, for a full exploitation of the FD recovery phase, the role of drift cannot be neglected (see, *e.g.,* Luo et al., 2018) but, as shown in Section 4, it is probably a second order correction. Therefore, for the exploratory purpose of this paper, we will neglect this correction and left the drift term unmodified. Finally, we consider the value of K_0 evaluated on the long-term and time-dependent analysis (*i.e.,* reproducing the average flux on a Carrington rotation hosting the FD, see *e.g.,* Boschini et al., 2024, and reference therein) as a reference, then we evaluate how the diffusion parameter in the innermost region evolves during the FD using the methodology described in Section 3.

3. Numerical analysis

3.1. FD selection

In Aguilar et al. (2021), the AMS–02 collaboration released the measured daily spectra for protons from 2011 May 20 to 2019 October 29 in the rigidity range from 1 to 100 GV. Wang et al. (2023) applied a systematic analysis method, identifying 142 FD events: 47 FDs caused by interplanetary CMEs and 54 caused by CIRs (which can be considered respectively as sporadic and recurrent FDs as defined in, *e.g.,* Wawrzynczak and Alania, 2008). In their analysis, each FD is characterized by FD amplitude (evaluated as the relative maximum depletion at 2 GV), maximum affected rigidity (MAR, *i.e.,* the rigidity up to which FD effects are still significant), and the time delay of minimum flux depletion after the FD starts. For this study, we selected five FDs, summarized in Table 1, among those with FD amplitude $> 10\%$ and with a clear asymmetric shape (*i.e.,* with a recovery phase $\gg$ decrease phase). The number of selected FDs was an arbitrary choice to cover the full period of AMS–02 data and to demonstrate the feasibility of the study in a reasonable amount of time on a local GPU architecture.

3.2. Computational effort

The search was performed on a single server with three NVIDIA A–30 GPU cards. Using this study as a baseline for code performances, we evaluate a need of $\sim 4.3k$ GPU hours to compute the full 142 sample reported in Wang et al. (2023), by a linear extrapolation. Additional computational time would be needed by more complex search, including more free parameters (*e.g.,* computing separately perpendicular and parallel diffusion). Using the adaptive grid search technique, utilized for the K_0 parameter investigation, the computational time rises as $\sim N_{par}!$,

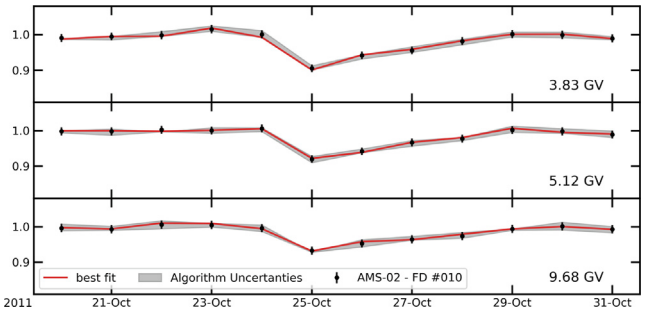

Fig. 1. Modulated differential intensities at 3.83, 5.12, and 9.68 GV during the FD 017. In each panel, black points are the daily values measured by AMS–02 with their experimental error. In red, we report the best-fit simulation for that day and rigidity, the gray area represents the uncertainties from the fit algorithm. All differential intensities are normalized to the average flux during the four days before the FD starts.

where N_{par} is the number of model free parameters. It reaches $\sim 25.8k$ GPU hours, becoming prohibitive, with just $N_{par} = 3$.

For such a simulation production, we suppose the use of the Bayesian Optimization (BO) parameter-tuning algorithm, because it demonstrated to be the best strategy for

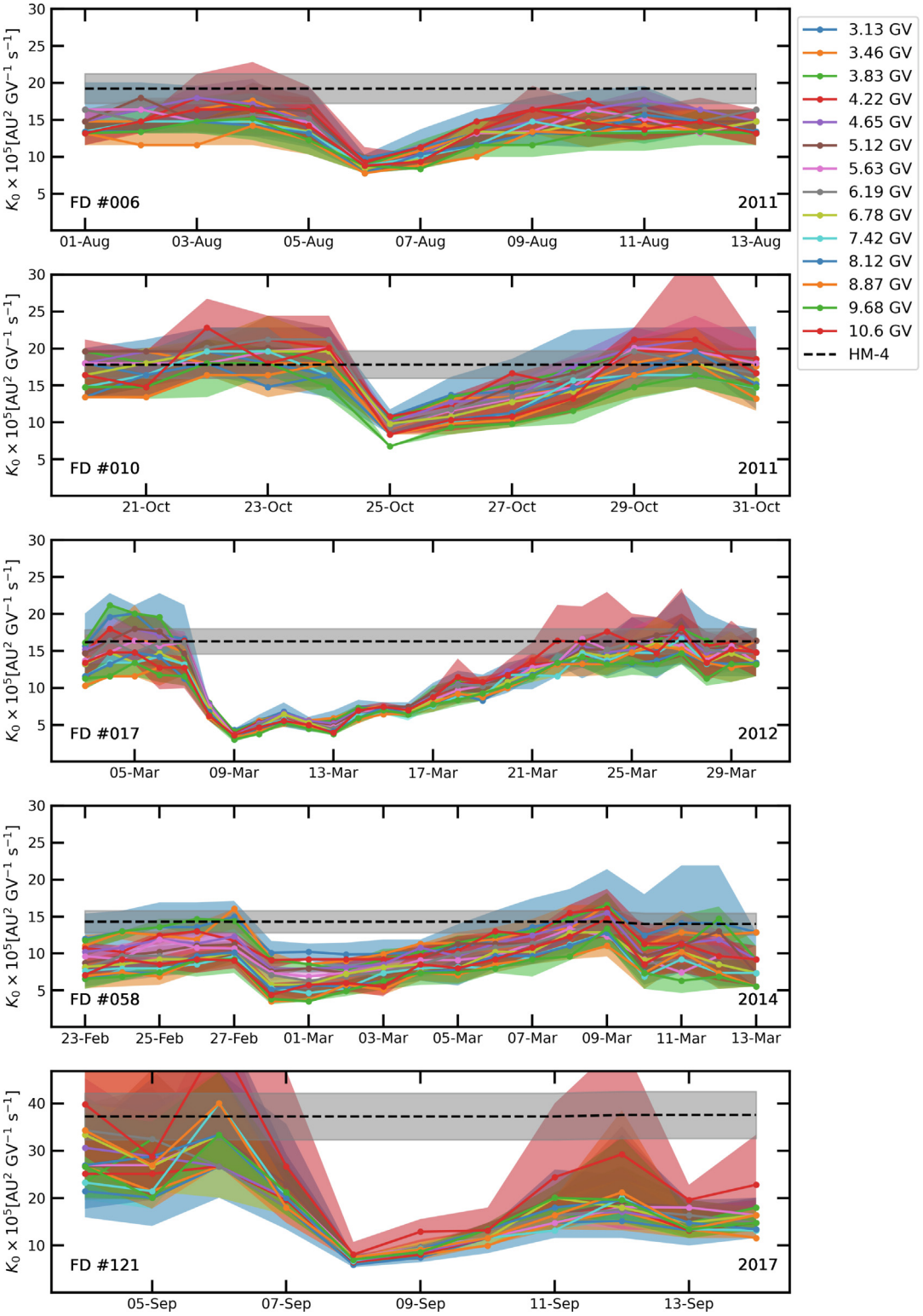

Fig. 2. Computed value of K_0 parameter for different days and several rigidities. The colored area represents the uncertainties on K_0 due to the fit algorithm. The black dashed line indicates the reference value of K_0 (along with the estimated uncertainties in the gray area) used in HELMOD-4/CUDA to reproduce the Carrington rotation average flux.

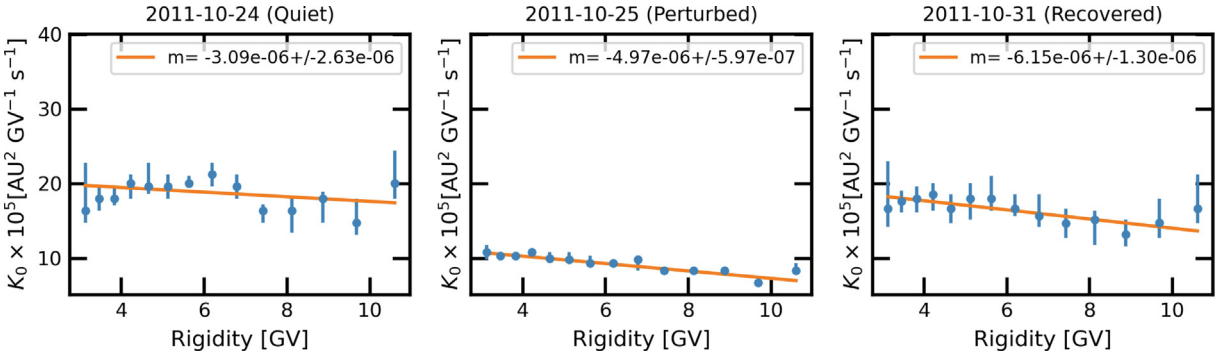

Fig. 3. Best-fit values of K_0 computed during FD #010, along with the computed uncertainties (blue points), for three selected days representing the initial (quiet) period (left panel), the day of the minimum flux (central panel), and the day after the recovering phase (right panel). Data are reported as a function of rigidity. The orange lines are the result of the linear fits of the plotted data, the slope of the fit is reported in the legend on top of each plot.

cases with low parameter dimensionality and few fitting points (see, *e.g.,* Balázs et al., 2021; Santoni et al., 2024; Roussel et al., 2024; Leclercq, 2018, for example of parameter search algorithm that may be used in this cases). Thus, the estimated computational time, can be computed applying the following approximation:

$$t_{BO} \simeq N_{BO}\,\langle x\rangle\, y + k\,N_{BO}^3 \tag{3}$$

where $N_{BO} \simeq 50$ is the number of evaluated samples for Gaussian process fitting, commonly used in literature (Mahendran et al., 2012; Falkner et al., 2018). In this work, $\langle x\rangle = 17$ is the average FD fitting points (days), $y = 212.0s$ is the average execution time for each day fitted, as extracted from the simulation profiling. $k = 0.1$s, instead, is the estimated time to evaluate a candidate function per fitting point, depending on the efficiency of the numerical libraries, hardware performance, and data structure overheads (see also Shahriari et al., 2016). Performing the BO and using a GPU-optimized version of the propagation algorithm[1], our estimation for, e.g., 10 free parameters and all the 142 Forbush is $\sim 30k$ GPU hours, which is below the limit of the resources dedicated to a medium size Italian SuperComputing Resource Allocation (ISCRA) project.

3.3. Simulation strategy

As a simulation strategy, AMS-02 (Aguilar et al., 2021) published daily proton fluxes and each day is simulated separately from the others using the parameters evaluated for the Carrington rotation that includes those days. Only the value of K_0 parameter in the first inner sector of HELMOD-4 heliosphere is changed and considered in this analysis. In HELMOD-4, K_0 sets the normalization of the overall contribution of flux diffusion to the particle transport in the heliosphere. This term includes (and somehow hides) any dependence of the diffusion term from the influence of turbulence on the local transport. In the attempt to highlight any hint of variation of the rigidity dependence of the spectral diffusion index in the PTE occurring in the very local heliosphere region after the shock (as suggested by, *e.g.,* Wawrzynczak and Alania, 2008), we decided to compute the best-fit value of K_0 for each rigidity bin separately and then compare them (see Section 4).

We performed an adaptive grid search strategy starting from an array of 10 values for K_0 in the interval $10^{-7} \sim 6 \times 10^{-4}$ [AU^2 GV^{-1} s^{-1}] which was recursively refined within a smaller interval until the simulated flux in each rigidity bin differed from experimental data for less than 1% (*i.e.,* corresponding to the numerical accuracy due to the number of simulated Monte Carlo events). The evaluation of the simulation accuracy is done separately for each rigidity, thus, in principle, the K_0 value minimizing the flux differences at a certain rigidity bin can be different from the value at another rigidity bin showing a possible hint of its rigidity dependence. Indeed, the minimizing procedure stops only when all rigidity bins are successfully minimized. The uncertainty of each K_0 value is defined as the interval for which the simulated flux falls inside the experimental uncertainties.

The simulation sample includes 4 days before the FD starts to serve as an unperturbed period to be compared with the perturbed ones. We simulated each day of the recovery phase of the FD until the flux returned to the same level as the unperturbed period. Data below 3 GV are not always available in the AMS–02 dataset due to orbit limitations, and therefore, we decided to exclude them from the simulation sample. We also excluded rigidities greater than 11 GV, which showed some convergence issues of the best-fit procedure during preliminary simulations. We reported in Fig. 1 an example of FD measured by AMS–02 at three different rigidities (*i.e.,* 3.83, 5.12, and 9,68 GV indicated with black points) along with the simulated spectra (red lines).

In Fig. 2 and A we report K_0 results from the fit algorithm along with the computed uncertainties. These results are discussed in Section 4.

[1] actually under development for the Italian Research Center on High-Performance Computing, Big Data and Quantum Computing (see Cavallotto et al., 2025, for preliminary results).

4. Results and discussions

The results of the numerical analysis (presented in Section 3) are summarized in Fig. 2. In these plots, we report the best-fit value of K_0 parameter for each simulated day and rigidity. The colored area represents the computed uncertainties from the fit algorithm. As a reference value, we report with a black dashed line the value of K_0 used in HELMOD-4/CUDA and computed using the equations in Boschini et al. (2018a, 2019, 2024) for the long-term solar modulation. It is worth remembering that K_0 represents the diffusion amplitude parameter, as a function of time, averaged over the first HELMOD zone (i.e., from 1 to 6–7 AU from the Sun). Therefore, it represents the weighted average between the actual diffusion parameter inside the perturbed region and that one applying to the quiet plasma conditions. As expected, the reference values match well with the quiet (unperturbed) periods, as well as when the

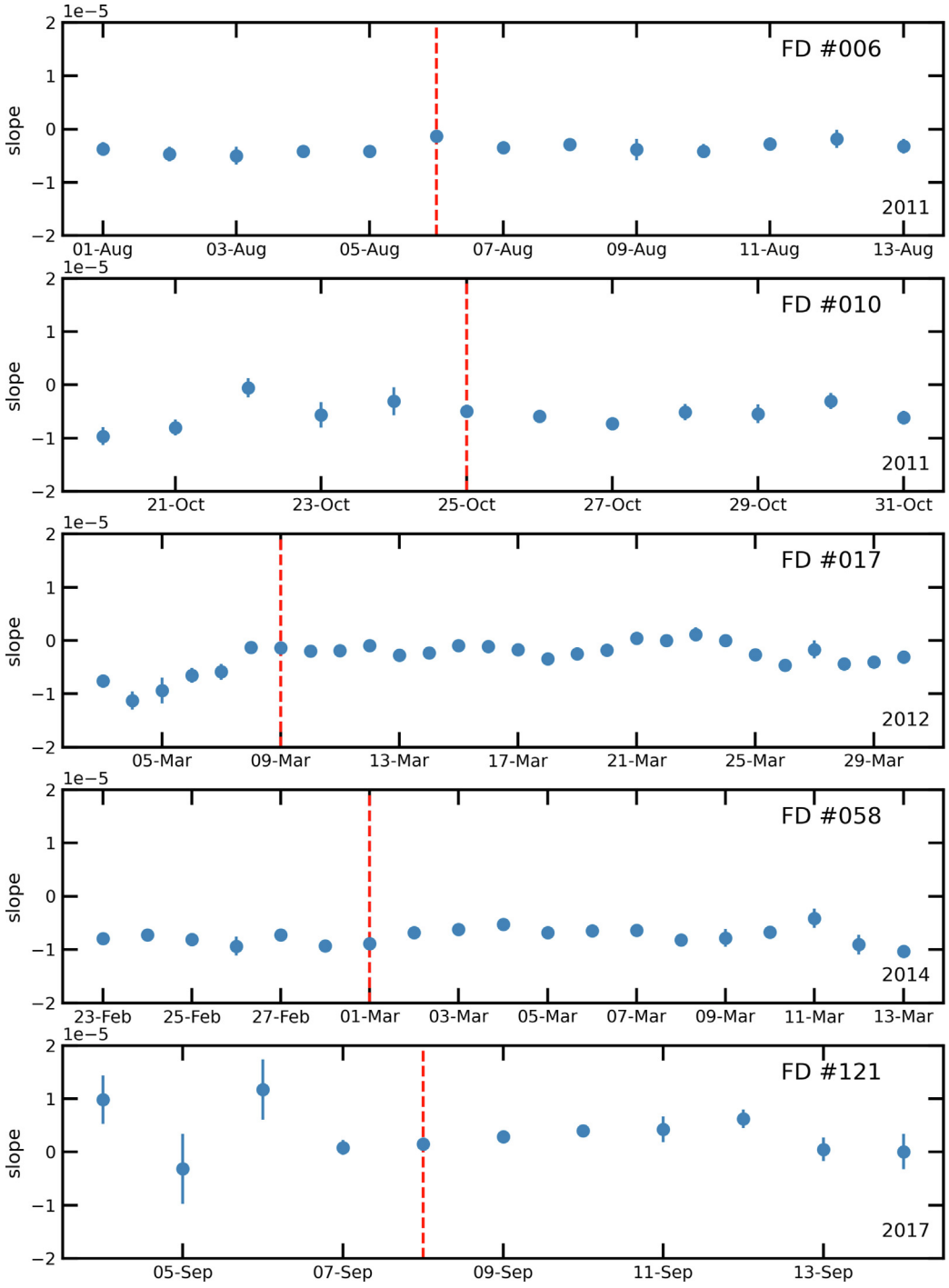

Fig. 4. Slope m in eq. (4) (i.e. rigidity dependence of K_0 with time) computed for the FDs considered in this study. The vertical dashed lines show the day of the FD onset as reported in Table 1.

flux is finally recovered, after FD, with the only exception of FD #121 case that remains below the initial (unperturbed) value. For the sake of discussion, we present in Fig. 3 a different view of results reported in tables in A, but for FD #010 only as a representative example. In these plots, we show the best-fit value of the K_0 parameter, as a function of rigidity, for three selected days, which represent the quiet (unperturbed) period, the day of the minimum flux, and the recovered flux (*i.e.,* the last day of the simulated period). From figure inspection, one can see how K_0 parameters seem to show a weak rigidity dependence that may reflect the need for improvements of the diffusion model (like, *e.g.,* a different rigidity dependence between parallel and perpendicular diffusion as presented in Engelbrecht et al., 2022 and reference there in), the need for a fine tune of the proton LIS or other effects related to transport near the heliosphere boundary. To see how this rigidity dependence varies during the FD evolution, we performed a linear regression (orange lines in Fig. 3) of K_0 parameters for each day with the general formula

$$K_0 = m \cdot P + a \tag{4}$$

where a and m are free parameters. The computed slope m is reported in Fig. 4 for the FDs in the present study. It is interesting to note that, in general, there is no significant variation before and after the beginning of the FD (indicated with vertical red dashed line). For the case of FD #017, during the quiet period, the slope constantly increases in the days before the onset of the FD. Thus, this change may not be related to the FD itself. A different feature is observed for FD #121 when the days during the quiet period show a large variability that disappears the day before the FD starts. In general, it is challenging to infer any structure that can be correlated with the evolution of the FD. This observation suggests that a) the rigidity dependence noticed in Fig. 3, and in all studied FDs, is a feature that is independent of the perturbed conditions during the FD, and b) the rigidity dependence of the diffusion coefficient (see eq. (2)) is not modified during the five studied FDs. In fact, if the rigidity dependence in eq. (2) is substantially modified during the FD evolution, this should be reflected in the computed value of K_0 best-fit values, which is not observed. This conclusion is not necessarily in contrast with those stated in Wawrzynczak and Alania (2008, 2010) because they focused their study on *recurrent* FDs, and the variation of the spectral index of the rigidity dependence may be so small that, in this study, it may be confused with typical fluctuations of an unmodified scenario.

5. Conclusion

In this work, we applied a modified version of HELMOD-4/CUDA code to the study of the temporal evolution of FDs. We developed a simple recursive algorithm to fit the diffusion parameter in the first inner region of the heliosphere to emulate the change in the diffusion process due to the large perturbations occurring during FD. We found that the same description of the diffusion coefficients with rigidity, used during the quiet period is suitable to reproduce the perturbed period in the five cases considered in this study. For each day, the value of the K_0 parameter is almost consistent among the considered rigidities. We found a residual linear rigidity dependence of the computed K_0 parameter that occurs both during quiet and perturbed periods. This may reflect an incorrect rigidity dependence of parallel and/or perpendicular diffusion tensor used in the current model. Finally, although the absolute value of the K_0 parameter varies significantly during the time evolution of the FD, it remains almost constant versus rigidity for both quiet and perturbed days. These observations support the idea that turbulence occurring during an FD event, while presenting much larger amplitudes in comparison with quiet periods, does not modify the general properties of particle propagation of GCR. The present study is limited by the low number of FD events considered and a very simplified spatial description of the FD itself. A more accurate description of the spatial evolution of the FD may help in recovering the differences observed among different events. For a more robust outcome, a wider investigation using many more FD events (including the study of helium nuclei and electrons, which are made available from AMS-02 in Aguilar et al., 2022; Aguilar et al., 2023) is requested. Since the volume probed by a solar eruption is much more localized than the global heliosphere, it may be more easily inspected with *in situ* probes. The study of the temporal evolution of FD may allow testing properties of particle propagation in a more known environment that can be simulated directly in the code. This possibility could help to disentangle different effects in GCR transport and, thus, to improve the modelization of the whole heliosphere.

Declaration of Competing Interest

The authors declare that they have no known competing financial interests or personal relationships that could have appeared to influence the work reported in this paper.

Acknowledgments

This paper is supported by the Fondazione ICSC, Spoke 3 Astrophysics and Cosmos Observations. National Recovery and Resilience Plan (Piano Nazionale di Ripresa e Resilienza, PNRR) Project ID CN_00000013 ”Italian Research Center on High-Performance Computing, Big Data and Quantum Computing” funded by MUR Missione 4 Componente 2 Investimento 1.4: Potenziamento strutture di ricerca e creazione di ”campioni nazionali di R&S (M4C2-19)” - Next Generation EU (NGEU) MG, SDT and GLV are supported by INFN and ASI under ASI-INFN Agreement No. 2019–19-HH.0 and its amendments and by ASIF implementation agreement No. 2021–36-HH.0 involving ASI and Milano-Bicocca University.

Appendix A. Tables

In the following tables, we report the values of computed daily K_0 parameters (expressed in $AU^2\,GV^{-1}s^{-1}$) for each simulated rigidity. Reported values in tables must be multiplied by 10^{-4}.

Table A.2. Daily $K_0 \times 10^{-4}$ parameter in $AU^2\,GV^{-1}s^{-1}$ during FD#006.

Day	3.13 GV	3.46 GV	3.83 GV	4.22 GV	4.65 GV	5.12 GV	5.63 GV
2011–08-01	$1.64^{+0.37}_{-0.32}$	$1.48^{+0.07}_{-0.07}$	$1.48^{+0.16}_{-0.16}$	$1.64^{+0.08}_{-0.16}$	$1.48^{+0.16}_{-0.07}$	$1.48^{+0.07}_{-0.16}$	$1.64^{+0.08}_{-0.30}$
2011–08-02	$1.64^{+0.37}_{-0.32}$	$1.48^{+0.16}_{-0.07}$	$1.64^{+0.08}_{-0.08}$	$1.48^{+0.16}_{-0.07}$	$1.64^{+0.08}_{-0.08}$	$1.80^{+0.09}_{-0.16}$	$1.64^{+0.08}_{-0.16}$
2011–08-03	$1.48^{+0.48}_{-0.16}$	$1.64^{+0.16}_{-0.08}$	$1.80^{+0.09}_{-0.16}$	$1.80^{+0.09}_{-0.16}$	$1.80^{+0.16}_{-0.16}$	$1.48^{+0.16}_{-0.07}$	$1.48^{+0.32}_{-0.07}$
2011–08-04	$1.52^{+0.39}_{-0.24}$	$1.76^{+0.05}_{-0.24}$	$1.66^{+0.14}_{-0.10}$	$1.64^{+0.22}_{-0.16}$	$1.71^{+0.34}_{-0.24}$	$1.66^{+0.34}_{-0.05}$	$1.57^{+0.15}_{-0.10}$
2011–08-05	$1.47^{+0.49}_{-0.19}$	$1.48^{+0.09}_{-0.06}$	$1.48^{+0.28}_{-0.01}$	$1.64^{+0.16}_{-0.17}$	$1.47^{+0.05}_{-0.15}$	$1.62^{+0.19}_{-0.19}$	$1.47^{+0.24}_{-0.15}$
2011–08-06	$0.98^{+0.05}_{-0.15}$	$0.88^{+0.04}_{-0.10}$	$0.88^{+0.05}_{-0.04}$	$0.93^{+0.05}_{-0.09}$	$0.84^{+0.09}_{-0.04}$	$0.88^{+0.04}_{-0.04}$	$0.88^{+0.10}_{-0.05}$
2011–08-07	$1.13^{+0.24}_{-0.15}$	$1.08^{+0.08}_{-0.05}$	$1.13^{+0.10}_{-0.05}$	$1.13^{+0.03}_{-0.10}$	$1.03^{+0.15}_{-0.03}$	$1.00^{+0.08}_{-0.01}$	$1.00^{+0.16}_{-0.01}$
2011–08-08	$1.32^{+0.32}_{-0.07}$	$1.32^{+0.02}_{-0.07}$	$1.48^{+0.07}_{-0.14}$	$1.48^{+0.07}_{-0.16}$	$1.32^{+0.07}_{-0.07}$	$1.34^{+0.07}_{-0.02}$	$1.32^{+0.02}_{-0.07}$
2011–08-09	$1.32^{+0.48}_{-0.07}$	$1.32^{+0.16}_{-0.07}$	$1.64^{+0.08}_{-0.16}$	$1.64^{+0.08}_{-0.08}$	$1.48^{+0.07}_{-0.07}$	$1.34^{+0.30}_{-0.02}$	$1.34^{+0.14}_{-0.02}$
2011–08-10	$1.48^{+0.43}_{-0.20}$	$1.47^{+0.17}_{-0.07}$	$1.62^{+0.10}_{-0.15}$	$1.76^{+0.09}_{-0.39}$	$1.64^{+0.07}_{-0.16}$	$1.47^{+0.24}_{-0.07}$	$1.64^{+0.03}_{-0.27}$
2011–08-11	$1.47^{+0.49}_{-0.24}$	$1.52^{+0.12}_{-0.05}$	$1.57^{+0.15}_{-0.10}$	$1.48^{+0.23}_{-0.06}$	$1.76^{+0.15}_{-0.19}$	$1.62^{+0.19}_{-0.19}$	$1.52^{+0.15}_{-0.20}$
2011–08-12	$1.48^{+0.16}_{-0.16}$	$1.34^{+0.14}_{-0.07}$	$1.48^{+0.16}_{-0.07}$	$1.48^{+0.07}_{-0.07}$	$1.64^{+0.08}_{-0.08}$	$1.48^{+0.07}_{-0.07}$	$1.32^{+0.07}_{-0.07}$
2011–08-13	$1.34^{+0.30}_{-0.02}$	$1.48^{+0.07}_{-0.16}$	$1.48^{+0.16}_{-0.07}$	$1.64^{+0.08}_{-0.16}$	$1.48^{+0.07}_{-0.07}$	$1.48^{+0.07}_{-0.14}$	$1.48^{+0.16}_{-0.07}$
Day	6.19 GV	6.78 GV	7.42 GV	8.12 GV	8.87 GV	9.68 GV	10.6 GV
2011–08-01	$1.64^{+0.08}_{-0.08}$	$1.32^{+0.16}_{-0.07}$	$1.34^{+0.14}_{-0.18}$	$1.34^{+0.14}_{-0.02}$	$1.32^{+0.02}_{-0.16}$	$1.32^{+0.16}_{-0.07}$	$1.32^{+0.16}_{-0.16}$
2011–08-02	$1.48^{+0.32}_{-0.07}$	$1.48^{+0.16}_{-0.07}$	$1.48^{+0.16}_{-0.14}$	$1.34^{+0.14}_{-0.02}$	$1.16^{+0.18}_{-0.06}$	$1.34^{+0.14}_{-0.02}$	$1.48^{+0.07}_{-0.16}$
2011–08-03	$1.48^{+0.32}_{-0.07}$	$1.48^{+0.16}_{-0.14}$	$1.48^{+0.32}_{-0.07}$	$1.48^{+0.16}_{-0.14}$	$1.16^{+0.32}_{-0.06}$	$1.48^{+0.07}_{-0.16}$	$1.64^{+0.48}_{-0.16}$
2011–08-04	$1.57^{+0.34}_{-0.10}$	$1.48^{+0.16}_{-0.16}$	$1.47^{+0.39}_{-0.15}$	$1.42^{+0.39}_{-0.15}$	$1.42^{+0.34}_{-0.26}$	$1.52^{+0.24}_{-0.29}$	$1.64^{+0.64}_{-0.22}$
2011–08-05	$1.52^{+0.15}_{-0.20}$	$1.34^{+0.14}_{-0.12}$	$1.32^{+0.24}_{-0.17}$	$1.32^{+0.10}_{-0.19}$	$1.23^{+0.12}_{-0.19}$	$1.23^{+0.12}_{-0.19}$	$1.42^{+0.54}_{-0.19}$
2011–08-06	$0.83^{+0.10}_{-0.05}$	$0.84^{+0.09}_{-0.01}$	$0.88^{+0.04}_{-0.05}$	$0.78^{+0.15}_{-0.04}$	$0.78^{+0.10}_{-0.04}$	$0.88^{+0.15}_{-0.10}$	$0.88^{+0.25}_{-0.05}$
2011–08-07	$0.98^{+0.15}_{-0.05}$	$0.98^{+0.05}_{-0.05}$	$1.00^{+0.05}_{-0.16}$	$1.03^{+0.05}_{-0.19}$	$0.88^{+0.10}_{-0.05}$	$0.84^{+0.10}_{-0.04}$	$0.93^{+0.10}_{-0.10}$
2011–08-08	$1.34^{+0.07}_{-0.18}$	$1.34^{+0.14}_{-0.02}$	$1.16^{+0.18}_{-0.06}$	$1.16^{+0.18}_{-0.06}$	$1.00^{+0.16}_{-0.05}$	$1.16^{+0.16}_{-0.16}$	$1.34^{+0.07}_{-0.18}$
2011–08-09	$1.64^{+0.08}_{-0.32}$	$1.32^{+0.16}_{-0.07}$	$1.48^{+0.16}_{-0.16}$	$1.32^{+0.16}_{-0.16}$	$1.34^{+0.30}_{-0.02}$	$1.16^{+0.16}_{-0.16}$	$1.64^{+0.32}_{-0.32}$
2011–08-10	$1.47^{+0.24}_{-0.15}$	$1.48^{+0.19}_{-0.16}$	$1.34^{+0.18}_{-0.07}$	$1.32^{+0.16}_{-0.19}$	$1.32^{+0.16}_{-0.19}$	$1.32^{+0.25}_{-0.24}$	$1.47^{+0.24}_{-0.19}$
2011–08-11	$1.64^{+0.16}_{-0.30}$	$1.37^{+0.19}_{-0.19}$	$1.34^{+0.18}_{-0.16}$	$1.57^{+0.15}_{-0.29}$	$1.42^{+0.19}_{-0.19}$	$1.32^{+0.10}_{-0.24}$	$1.37^{+0.29}_{-0.15}$
2011–08-12	$1.48^{+0.07}_{-0.07}$	$1.34^{+0.30}_{-0.07}$	$1.34^{+0.14}_{-0.02}$	$1.48^{+0.07}_{-0.16}$	$1.34^{+0.30}_{-0.02}$	$1.34^{+0.30}_{-0.18}$	$1.48^{+0.32}_{-0.16}$
2011–08-13	$1.64^{+0.08}_{-0.08}$	$1.48^{+0.07}_{-0.16}$	$1.32^{+0.16}_{-0.07}$	$1.32^{+0.16}_{-0.07}$	$1.32^{+0.02}_{-0.16}$	$1.32^{+0.16}_{-0.16}$	$1.32^{+0.32}_{-0.16}$

Table A.3. Daily $K_0 \times 10^{-4}$ parameter in $AU^2\,GV^{-1}s^{-1}$ during FD#010.

Day	3.13 GV	3.46 GV	3.83 GV	4.22 GV	4.65 GV	5.12 GV	5.63 GV
2011–10-20	$1.80^{+0.21}_{-0.46}$	$1.80^{+0.09}_{-0.09}$	$1.96^{+0.10}_{-0.32}$	$1.80^{+0.09}_{-0.16}$	$1.80^{+0.09}_{-0.16}$	$1.96^{+0.10}_{-0.16}$	$1.80^{+0.21}_{-0.09}$
2011–10-21	$1.64^{+0.48}_{-0.16}$	$1.96^{+0.10}_{-0.16}$	$1.80^{+0.09}_{-0.16}$	$1.96^{+0.10}_{-0.10}$	$1.96^{+0.10}_{-0.32}$	$1.96^{+0.05}_{-0.16}$	$1.80^{+0.16}_{-0.16}$
2011–10-22	$1.96^{+0.32}_{-0.32}$	$1.80^{+0.21}_{-0.09}$	$1.80^{+0.16}_{-0.09}$	$1.96^{+0.10}_{-0.10}$	$1.96^{+0.16}_{-0.16}$	$1.96^{+0.05}_{-0.16}$	$1.80^{+0.21}_{-0.09}$
2011–10-23	$1.80^{+0.48}_{-0.32}$	$1.80^{+0.16}_{-0.09}$	$2.01^{+0.28}_{-0.05}$	$2.12^{+0.11}_{-0.16}$	$1.96^{+0.32}_{-0.10}$	$2.01^{+0.11}_{-0.21}$	$1.96^{+0.32}_{-0.16}$

(*continued on next page*)

Table A.3 (*continued*)

Day	3.13 GV	3.46 GV	3.83 GV	4.22 GV	4.65 GV	5.12 GV	5.63 GV
2011–10-24	$1.64^{+0.64}_{-0.16}$	$1.80^{+0.16}_{-0.16}$	$1.80^{+0.16}_{-0.09}$	$2.01^{+0.11}_{-0.21}$	$1.96^{+0.32}_{-0.10}$	$1.96^{+0.16}_{-0.16}$	$2.01^{+0.10}_{-0.05}$
2011–10-25	$1.08^{+0.10}_{-0.10}$	$1.03^{+0.05}_{-0.03}$	$1.03^{+0.05}_{-0.05}$	$1.08^{+0.05}_{-0.08}$	$1.00^{+0.08}_{-0.06}$	$0.98^{+0.10}_{-0.05}$	$0.93^{+0.10}_{-0.05}$
2011–10-26	$1.37^{+0.24}_{-0.29}$	$1.32^{+0.05}_{-0.05}$	$1.34^{+0.07}_{-0.16}$	$1.23^{+0.15}_{-0.06}$	$1.27^{+0.07}_{-0.10}$	$1.16^{+0.07}_{-0.03}$	$1.16^{+0.16}_{-0.03}$
2011–10-27	$1.42^{+0.44}_{-0.15}$	$1.34^{+0.18}_{-0.02}$	$1.52^{+0.05}_{-0.19}$	$1.66^{+0.08}_{-0.24}$	$1.32^{+0.24}_{-0.01}$	$1.48^{+0.04}_{-0.16}$	$1.32^{+0.20}_{-0.09}$
2011–10-28	$1.47^{+0.78}_{-0.24}$	$1.48^{+0.19}_{-0.06}$	$1.71^{+0.05}_{-0.23}$	$1.48^{+0.38}_{-0.11}$	$1.76^{+0.15}_{-0.28}$	$1.66^{+0.08}_{-0.19}$	$1.48^{+0.38}_{-0.01}$
2011–10-29	$1.80^{+0.48}_{-0.32}$	$1.80^{+0.09}_{-0.09}$	$1.96^{+0.05}_{-0.32}$	$1.96^{+0.05}_{-0.16}$	$2.01^{+0.28}_{-0.21}$	$1.96^{+0.16}_{-0.16}$	$2.01^{+0.11}_{-0.21}$
2011–10-30	$1.80^{+0.48}_{-0.16}$	$1.96^{+0.05}_{-0.16}$	$1.96^{+0.16}_{-0.16}$	$1.96^{+0.05}_{-0.16}$	$2.12^{+0.11}_{-0.32}$	$1.80^{+0.16}_{-0.16}$	$1.96^{+0.48}_{-0.10}$
2011–10-31	$1.66^{+0.63}_{-0.24}$	$1.76^{+0.15}_{-0.15}$	$1.80^{+0.16}_{-0.18}$	$1.86^{+0.15}_{-0.22}$	$1.66^{+0.19}_{-0.19}$	$1.80^{+0.21}_{-0.28}$	$1.80^{+0.30}_{-0.16}$
Day	6.19 GV	6.78 GV	7.42 GV	8.12 GV	8.87 GV	9.68 GV	10.6 GV
2011–10-20	$1.64^{+0.32}_{-0.16}$	$1.64^{+0.16}_{-0.16}$	$1.48^{+0.32}_{-0.16}$	$1.34^{+0.14}_{-0.02}$	$1.34^{+0.46}_{-0.07}$	$1.48^{+0.48}_{-0.14}$	$1.64^{+0.48}_{-0.30}$
2011–10-21	$1.80^{+0.21}_{-0.16}$	$1.80^{+0.21}_{-0.09}$	$1.64^{+0.32}_{-0.16}$	$1.64^{+0.16}_{-0.16}$	$1.34^{+0.30}_{-0.02}$	$1.48^{+0.16}_{-0.16}$	$1.48^{+0.48}_{-0.16}$
2011–10-22	$2.01^{+0.10}_{-0.37}$	$1.96^{+0.16}_{-0.16}$	$1.96^{+0.32}_{-0.16}$	$1.80^{+0.32}_{-0.09}$	$1.64^{+0.37}_{-0.08}$	$1.80^{+0.32}_{-0.46}$	$2.28^{+0.39}_{-0.64}$
2011–10-23	$2.12^{+0.32}_{-0.16}$	$1.96^{+0.48}_{-0.10}$	$1.96^{+0.32}_{-0.16}$	$1.48^{+0.16}_{-0.07}$	$1.64^{+0.37}_{-0.30}$	$1.80^{+0.21}_{-0.16}$	$1.80^{+0.64}_{-0.16}$
2011–10-24	$2.12^{+0.16}_{-0.16}$	$1.96^{+0.16}_{-0.16}$	$1.64^{+0.08}_{-0.16}$	$1.64^{+0.16}_{-0.30}$	$1.80^{+0.09}_{-0.32}$	$1.48^{+0.32}_{-0.16}$	$2.01^{+0.44}_{-0.21}$
2011–10-25	$0.93^{+0.05}_{-0.05}$	$0.98^{+0.05}_{-0.15}$	$0.84^{+0.05}_{-0.04}$	$0.84^{+0.05}_{-0.04}$	$0.84^{+0.04}_{-0.04}$	$0.68^{+0.03}_{-0.03}$	$0.84^{+0.10}_{-0.04}$
2011–10-26	$1.18^{+0.16}_{-0.05}$	$1.08^{+0.10}_{-0.10}$	$1.00^{+0.13}_{-0.06}$	$1.03^{+0.10}_{-0.10}$	$0.98^{+0.05}_{-0.15}$	$0.93^{+0.06}_{-0.10}$	$1.03^{+0.15}_{-0.15}$
2011–10-27	$1.34^{+0.08}_{-0.12}$	$1.27^{+0.10}_{-0.15}$	$1.13^{+0.21}_{-0.05}$	$1.13^{+0.10}_{-0.15}$	$1.03^{+0.29}_{-0.10}$	$0.98^{+0.15}_{-0.05}$	$1.08^{+0.24}_{-0.10}$
2011–10-28	$1.62^{+0.18}_{-0.15}$	$1.42^{+0.24}_{-0.10}$	$1.57^{+0.24}_{-0.29}$	$1.47^{+0.19}_{-0.29}$	$1.32^{+0.15}_{-0.19}$	$1.16^{+0.18}_{-0.18}$	$1.32^{+0.29}_{-0.19}$
2011–10-29	$1.96^{+0.16}_{-0.32}$	$1.64^{+0.16}_{-0.08}$	$1.64^{+0.16}_{-0.16}$	$1.64^{+0.16}_{-0.16}$	$1.64^{+0.37}_{-0.30}$	$1.48^{+0.07}_{-0.16}$	$2.12^{+0.16}_{-0.48}$
2011–10-30	$1.80^{+0.48}_{-0.09}$	$1.80^{+0.21}_{-0.16}$	$1.64^{+0.37}_{-0.16}$	$1.96^{+0.16}_{-0.16}$	$1.80^{+0.48}_{-0.32}$	$1.64^{+0.37}_{-0.16}$	$2.12^{+1.22}_{-0.32}$
2011–10-31	$1.66^{+0.19}_{-0.10}$	$1.57^{+0.29}_{-0.15}$	$1.47^{+0.19}_{-0.19}$	$1.52^{+0.12}_{-0.34}$	$1.32^{+0.19}_{-0.17}$	$1/.48^{+0.32}_{-0.20}$	$1.66^{+0.46}_{-0.19}$

Table A.4. Daily $K_0 \times 10^{-4}$ parameter in $AU^2 GV^{-1} s^{-1}$ during FD#017.

Day	3.13 GV	3.46 GV	3.83 GV	4.22 GV	4.65 GV	5.12 GV	5.63 GV
2012–03-03	$1.57^{+0.44}_{-0.29}$	$1.47^{+0.24}_{-0.07}$	$1.62^{+0.05}_{-0.24}$	$1.48^{+0.09}_{-0.11}$	$1.52^{+0.12}_{-0.10}$	$1.47^{+0.10}_{-0.15}$	$1.37^{+0.19}_{-0.05}$
2012–03-04	$1.96^{+0.32}_{-0.32}$	$1.80^{+0.09}_{-0.09}$	$2.12^{+0.11}_{-0.16}$	$1.80^{+0.09}_{-0.16}$	$1.64^{+0.37}_{-0.08}$	$1.64^{+0.16}_{-0.08}$	$1.48^{+0.16}_{-0.07}$
2012–03-05	$2.01^{+0.11}_{-0.37}$	$1.64^{+0.48}_{-0.08}$	$2.01^{+0.10}_{-0.21}$	$1.64^{+0.16}_{-0.08}$	$1.80^{+0.09}_{-0.09}$	$1.80^{+0.21}_{-0.16}$	$1.64^{+0.16}_{-0.08}$
2012–03-06	$1.71^{+0.57}_{-0.29}$	$1.62^{+0.10}_{-0.05}$	$1.96^{+0.10}_{-0.29}$	$1.57^{+0.24}_{-0.08}$	$1.71^{+0.10}_{-0.24}$	$1.76^{+0.19}_{-0.15}$	$1.57^{+0.24}_{-0.15}$
2012–03-07	$1.66^{+0.46}_{-0.29}$	$1.48^{+0.19}_{-0.01}$	$1.42^{+0.24}_{-0.07}$	$1.64^{+0.07}_{-0.17}$	$1.62^{+0.15}_{-0.10}$	$1.47^{+0.15}_{-0.10}$	$1.62^{+0.15}_{-0.27}$
2012–03-08	$0.68^{+0.11}_{-0.07}$	$0.68^{+0.02}_{-0.04}$	$0.80^{+0.02}_{-0.11}$	$0.77^{+0.05}_{-0.02}$	$0.78^{+0.07}_{-0.09}$	$0.75^{+0.09}_{-0.00}$	$0.75^{+0.07}_{-0.05}$
2012–03-09	$0.43^{+0.02}_{-0.05}$	$0.38^{+0.04}_{-0.02}$	$0.41^{+0.02}_{-0.04}$	$0.38^{+0.02}_{-0.00}$	$0.36^{+0.02}_{-0.02}$	$0.36^{+0.04}_{-0.02}$	$0.36^{+0.02}_{-0.04}$
2012–03-10	$0.56^{+0.08}_{-0.05}$	$0.56^{+0.03}_{-0.04}$	$0.54^{+0.05}_{-0.03}$	$0.54^{+0.03}_{-0.02}$	$0.52^{+0.04}_{-0.03}$	$0.45^{+0.07}_{-0.02}$	$0.48^{+0.04}_{-0.01}$
2012–03-11	$0.68^{+0.12}_{-0.05}$	$0.64^{+0.06}_{-0.03}$	$0.64^{+0.03}_{-0.02}$	$0.61^{+0.02}_{-0.03}$	$0.66^{+0.04}_{-0.02}$	$0.64^{+0.00}_{-0.05}$	$0.63^{+0.03}_{-0.07}$
2012–03-12	$0.56^{+0.05}_{-0.08}$	$0.56^{+0.03}_{-0.03}$	$0.53^{+0.01}_{-0.03}$	$0.50^{+0.03}_{-0.03}$	$0.56^{+0.03}_{-0.05}$	$0.53^{+0.05}_{-0.01}$	$0.52^{+0.05}_{-0.05}$
2012–03-13	$0.57^{+0.12}_{-0.07}$	$0.59^{+0.03}_{-0.04}$	$0.56^{+0.05}_{-0.03}$	$0.53^{+0.06}_{-0.01}$	$0.52^{+0.04}_{-0.03}$	$0.48^{+0.05}_{-0.04}$	$0.47^{+0.06}_{-0.02}$
2012–03-14	$0.73^{+0.11}_{-0.09}$	$0.71^{+0.04}_{-0.02}$	$0.73^{+0.04}_{-0.06}$	$0.68^{+0.07}_{-0.03}$	$0.70^{+0.07}_{-0.04}$	$0.68^{+0.02}_{-0.04}$	$0.64^{+0.04}_{-0.05}$
2012–03-15	$0.74^{+0.06}_{-0.07}$	$0.75^{+0.04}_{-0.04}$	$0.70^{+0.05}_{-0.03}$	$0.74^{+0.01}_{-0.04}$	$0.68^{+0.08}_{-0.03}$	$0.75^{+0.04}_{-0.01}$	$0.75^{+0.04}_{-0.05}$
2012–03-16	$0.74^{+0.06}_{-0.07}$	$0.70^{+0.03}_{-0.03}$	$0.70^{+0.05}_{-0.02}$	$0.70^{+0.05}_{-0.02}$	$0.74^{+0.01}_{-0.05}$	$0.74^{+0.04}_{-0.10}$	$0.68^{+0.02}_{-0.03}$

Table A.4 (*continued*)

Day	3.13 GV	3.46 GV	3.83 GV	4.22 GV	4.65 GV	5.12 GV	5.63 GV
2012–03-17	$0.87^{+0.20}_{-0.08}$	$0.87^{+0.08}_{-0.05}$	$0.89^{+0.14}_{-0.06}$	$0.88^{+0.01}_{-0.04}$	$0.91^{+0.02}_{-0.07}$	$0.94^{+0.05}_{-0.08}$	$0.84^{+0.09}_{-0.04}$
2012–03-18	$1.07^{+0.16}_{-0.21}$	$1.09^{+0.04}_{-0.11}$	$1.08^{+0.04}_{-0.10}$	$1.05^{+0.05}_{-0.08}$	$1.05^{+0.11}_{-0.07}$	$1.00^{+0.13}_{-0.05}$	$0.97^{+0.11}_{-0.09}$
2012–03-19	$1.03^{+0.15}_{-0.10}$	$1.03^{+0.13}_{-0.05}$	$1.03^{+0.05}_{-0.05}$	$1.08^{+0.08}_{-0.05}$	$1.03^{+0.05}_{-0.05}$	$1.03^{+0.05}_{-0.05}$	$1.03^{+0.05}_{-0.05}$
2012–03-20	$1.08^{+0.26}_{-0.10}$	$1.08^{+0.08}_{-0.08}$	$1.08^{+0.05}_{-0.05}$	$1.16^{+0.07}_{-0.03}$	$1.23^{+0.05}_{-0.15}$	$1.16^{+0.02}_{-0.08}$	$1.08^{+0.05}_{-0.05}$
2012–03-21	$1.32^{+0.10}_{-0.34}$	$1.16^{+0.06}_{-0.03}$	$1.16^{+0.16}_{-0.03}$	$1.32^{+0.07}_{-0.14}$	$1.27^{+0.19}_{-0.10}$	$1.23^{+0.10}_{-0.05}$	$1.27^{+0.10}_{-0.10}$
2012–03-22	$1.34^{+0.14}_{-0.18}$	$1.34^{+0.07}_{-0.02}$	$1.32^{+0.07}_{-0.07}$	$1.34^{+0.07}_{-0.02}$	$1.32^{+0.02}_{-0.07}$	$1.32^{+0.16}_{-0.07}$	$1.34^{+0.07}_{-0.02}$
2012–03-23	$1.32^{+0.35}_{-0.04}$	$1.32^{+0.16}_{-0.07}$	$1.37^{+0.05}_{-0.07}$	$1.42^{+0.15}_{-0.05}$	$1.57^{+0.05}_{-0.25}$	$1.52^{+0.12}_{-0.15}$	$1.66^{+0.08}_{-0.29}$
2012–03-24	$1.47^{+0.24}_{-0.31}$	$1.34^{+0.23}_{-0.07}$	$1.32^{+0.16}_{-0.01}$	$1.42^{+0.10}_{-0.05}$	$1.48^{+0.16}_{-0.06}$	$1.52^{+0.15}_{-0.18}$	$1.52^{+0.12}_{-0.19}$
2012–03-25	$1.52^{+0.44}_{-0.24}$	$1.62^{+0.05}_{-0.19}$	$1.57^{+0.24}_{-0.10}$	$1.48^{+0.23}_{-0.06}$	$1.52^{+0.44}_{-0.08}$	$1.62^{+0.18}_{-0.10}$	$1.62^{+0.19}_{-0.15}$
2012–03-26	$1.48^{+0.48}_{-0.35}$	$1.57^{+0.19}_{-0.15}$	$1.64^{+0.12}_{-0.07}$	$1.71^{+0.10}_{-0.24}$	$1.71^{+0.10}_{-0.19}$	$1.71^{+0.10}_{-0.15}$	$1.62^{+0.34}_{-0.10}$
2012–03-27	$1.76^{+0.54}_{-0.39}$	$1.57^{+0.15}_{-0.05}$	$1.80^{+0.01}_{-0.23}$	$1.66^{+0.15}_{-0.10}$	$1.71^{+0.19}_{-0.10}$	$1.76^{+0.24}_{-0.19}$	$1.57^{+0.24}_{-0.05}$
2012–03-28	$1.48^{+0.53}_{-0.20}$	$1.42^{+0.10}_{-0.05}$	$1.64^{+0.07}_{-0.17}$	$1.57^{+0.08}_{-0.15}$	$1.48^{+0.14}_{-0.16}$	$1.52^{+0.24}_{-0.05}$	$1.37^{+0.39}_{-0.07}$
2012–03-29	$1.57^{+0.29}_{-0.34}$	$1.47^{+0.17}_{-0.19}$	$1.47^{+0.19}_{-0.05}$	$1.62^{+0.10}_{-0.19}$	$1.52^{+0.10}_{-0.10}$	$1.57^{+0.10}_{-0.10}$	$1.57^{+0.07}_{-0.23}$
2012–03-30	$1.64^{+0.16}_{-0.32}$	$1.64^{+0.08}_{-0.16}$	$1.34^{+0.14}_{-0.07}$	$1.48^{+0.16}_{-0.07}$	$1.48^{+0.07}_{-0.07}$	$1.64^{+0.16}_{-0.16}$	$1.34^{+0.14}_{-0.07}$
Day	6.19 GV	6.78 GV	7.42 GV	8.12 GV	8.87 GV	9.68 GV	10.6 GV
2012–03-03	$1.32^{+0.10}_{-0.07}$	$1.32^{+0.10}_{-0.05}$	$1.16^{+0.16}_{-0.03}$	$1.16^{+0.18}_{-0.08}$	$1.03^{+0.19}_{-0.05}$	$1.13^{+0.19}_{-0.15}$	$1.34^{+0.14}_{-0.26}$
2012–03-04	$1.64^{+0.08}_{-0.16}$	$1.48^{+0.07}_{-0.16}$	$1.34^{+0.14}_{-0.02}$	$1.32^{+0.16}_{-0.16}$	$1.16^{+0.18}_{-0.06}$	$1.16^{+0.18}_{-0.06}$	$1.48^{+0.32}_{-0.07}$
2012–03-05	$1.48^{+0.07}_{-0.07}$	$1.34^{+0.07}_{-0.02}$	$1.34^{+0.14}_{-0.02}$	$1.48^{+0.07}_{-0.14}$	$1.16^{+0.18}_{-0.06}$	$1.34^{+0.07}_{-0.18}$	$1.48^{+0.16}_{-0.16}$
2012–03-06	$1.62^{+0.02}_{-0.15}$	$1.47^{+0.19}_{-0.15}$	$1.42^{+0.10}_{-0.15}$	$1.42^{+0.22}_{-0.15}$	$1.27^{+0.15}_{-0.24}$	$1.18^{+0.19}_{-0.10}$	$1.27^{+0.19}_{-0.29}$
2012–03-07	$1.62^{+0.05}_{-0.27}$	$1.32^{+0.32}_{-0.04}$	$1.32^{+0.20}_{-0.14}$	$1.13^{+0.24}_{-0.06}$	$1.27^{+0.36}_{-0.10}$	$1.16^{+0.18}_{-0.13}$	$1.27^{+0.15}_{-0.28}$
2012–03-08	$0.69^{+0.09}_{-0.03}$	$0.71^{+0.04}_{-0.07}$	$0.64^{+0.05}_{-0.06}$	$0.68^{+0.07}_{-0.05}$	$0.61^{+0.07}_{-0.05}$	$0.64^{+0.06}_{-0.08}$	$0.62^{+0.05}_{-0.07}$
2012–03-09	$0.34^{+0.02}_{-0.02}$	$0.34^{+0.02}_{-0.02}$	$0.31^{+0.02}_{-0.02}$	$0.31^{+0.02}_{-0.02}$	$0.32^{+0.02}_{-0.02}$	$0.30^{+0.00}_{-0.04}$	$0.36^{+0.03}_{-0.04}$
2012–03-10	$0.50^{+0.02}_{-0.04}$	$0.47^{+0.01}_{-0.02}$	$0.47^{+0.02}_{-0.06}$	$0.47^{+0.02}_{-0.02}$	$0.41^{+0.06}_{-0.02}$	$0.38^{+0.07}_{-0.02}$	$0.47^{+0.07}_{-0.05}$
2012–03-11	$0.63^{+0.04}_{-0.04}$	$0.64^{+0.03}_{-0.11}$	$0.57^{+0.01}_{-0.09}$	$0.52^{+0.04}_{-0.05}$	$0.52^{+0.02}_{-0.05}$	$0.53^{+0.01}_{-0.04}$	$0.55^{+0.04}_{-0.04}$
2012–03-12	$0.53^{+0.01}_{-0.06}$	$0.53^{+0.01}_{-0.04}$	$0.48^{+0.05}_{-0.04}$	$0.45^{+0.04}_{-0.04}$	$0.48^{+0.02}_{-0.02}$	$0.45^{+0.08}_{-0.03}$	$0.50^{+0.02}_{-0.05}$
2012–03-13	$0.45^{+0.02}_{-0.02}$	$0.41^{+0.05}_{-0.02}$	$0.41^{+0.02}_{-0.02}$	$0.42^{+0.02}_{-0.02}$	$0.39^{+0.05}_{-0.02}$	$0.38^{+0.02}_{-0.02}$	$0.39^{+0.05}_{-0.02}$
2012–03-14	$0.64^{+0.09}_{-0.01}$	$0.59^{+0.05}_{-0.02}$	$0.64^{+0.05}_{-0.04}$	$0.59^{+0.02}_{-0.04}$	$0.57^{+0.04}_{-0.05}$	$0.59^{+0.09}_{-0.06}$	$0.69^{+0.06}_{-0.12}$
2012–03-15	$0.70^{+0.03}_{-0.03}$	$0.70^{+0.05}_{-0.02}$	$0.65^{+0.11}_{-0.03}$	$0.74^{+0.04}_{-0.07}$	$0.65^{+0.05}_{-0.03}$	$0.70^{+0.03}_{-0.05}$	$0.74^{+0.06}_{-0.10}$
2012–03-16	$0.65^{+0.03}_{-0.05}$	$0.68^{+0.03}_{-0.08}$	$0.65^{+0.03}_{-0.08}$	$0.65^{+0.03}_{-0.03}$	$0.65^{+0.05}_{-0.03}$	$0.65^{+0.05}_{-0.05}$	$0.70^{+0.05}_{-0.05}$
2012–03-17	$0.91^{+0.07}_{-0.13}$	$0.83^{+0.08}_{-0.10}$	$0.76^{+0.11}_{-0.02}$	$0.78^{+0.11}_{-0.03}$	$0.79^{+0.10}_{-0.12}$	$0.78^{+0.08}_{-0.10}$	$0.87^{+0.10}_{-0.10}$
2012–03-18	$1.04^{+0.09}_{-0.11}$	$0.89^{+0.09}_{-0.05}$	$0.89^{+0.11}_{-0.08}$	$0.92^{+0.10}_{-0.13}$	$0.92^{+0.07}_{-0.13}$	$0.84^{+0.10}_{-0.08}$	$1.15^{+0.25}_{-0.20}$
2012–03-19	$1.03^{+0.05}_{-0.10}$	$0.93^{+0.10}_{-0.05}$	$0.88^{+0.15}_{-0.04}$	$0.83^{+0.15}_{-0.04}$	$0.88^{+0.04}_{-0.05}$	$0.93^{+0.10}_{-0.10}$	$1.08^{+0.05}_{-0.15}$
2012–03-20	$1.08^{+0.08}_{-0.05}$	$1.08^{+0.10}_{-0.05}$	$1.18^{+0.05}_{-0.19}$	$1.03^{+0.05}_{-0.10}$	$1.00^{+0.08}_{-0.01}$	$1.03^{+0.13}_{-0.05}$	$1.18^{+0.19}_{-0.10}$
2012–03-21	$1.18^{+0.24}_{-0.06}$	$1.23^{+0.05}_{-0.15}$	$1.18^{+0.15}_{-0.05}$	$1.18^{+0.19}_{-0.05}$	$1.16^{+0.31}_{-0.06}$	$1.16^{+0.18}_{-0.08}$	$1.37^{+0.24}_{-0.24}$
2012–03-22	$1.32^{+0.02}_{-0.07}$	$1.32^{+0.16}_{-0.16}$	$1.16^{+0.18}_{-0.06}$	$1.34^{+0.14}_{-0.02}$	$1.32^{+0.02}_{-0.16}$	$1.34^{+0.07}_{-0.02}$	$1.64^{+0.48}_{-0.16}$
2012–03-23	$1.34^{+0.37}_{-0.07}$	$1.48^{+0.19}_{-0.16}$	$1.47^{+0.15}_{-0.15}$	$1.32^{+0.25}_{-0.19}$	$1.32^{+0.16}_{-0.17}$	$1.42^{+0.29}_{-0.15}$	$1.62^{+0.49}_{-0.24}$
2012–03-24	$1.52^{+0.24}_{-0.15}$	$1.42^{+0.06}_{-0.19}$	$1.37^{+0.15}_{-0.10}$	$1.34^{+0.37}_{-0.07}$	$1.32^{+0.20}_{-0.14}$	$1.32^{+0.16}_{-0.19}$	$1.76^{+0.54}_{-0.28}$
2012–03-25	$1.62^{+0.18}_{-0.15}$	$1.48^{+0.19}_{-0.14}$	$1.48^{+0.19}_{-0.20}$	$1.32^{+0.29}_{-0.05}$	$1.48^{+0.32}_{-0.16}$	$1.34^{+0.30}_{-0.16}$	$1.62^{+0.39}_{-0.19}$

(*continued on next page*)

Table A.4 (*continued*)

Day	3.13 GV	3.46 GV	3.83 GV	4.22 GV	4.65 GV	5.12 GV	5.63 GV
2012–03-26	$1.57^{+0.29}_{-0.08}$	$1.62^{+0.34}_{-0.05}$	$1.47^{+0.24}_{-0.10}$	$1.37^{+0.24}_{-0.10}$	$1.57^{+0.19}_{-0.29}$	$1.32^{+0.16}_{-0.16}$	$1.47^{+0.49}_{-0.15}$
2012–03-27	$1.80^{+0.21}_{-0.16}$	$1.52^{+0.28}_{-0.18}$	$1.66^{+0.19}_{-0.32}$	$1.48^{+0.48}_{-0.16}$	$1.52^{+0.24}_{-0.18}$	$1.47^{+0.44}_{-0.15}$	$1.81^{+0.54}_{-0.39}$
2012–03-28	$1.52^{+0.24}_{-0.10}$	$1.34^{+0.23}_{-0.02}$	$1.32^{+0.10}_{-0.17}$	$1.34^{+0.18}_{-0.18}$	$1.34^{+0.14}_{-0.18}$	$1.13^{+0.15}_{-0.10}$	$1.34^{+0.23}_{-0.26}$
2012–03-29	$1.47^{+0.29}_{-0.13}$	$1.47^{+0.29}_{-0.15}$	$1.32^{+0.16}_{-0.09}$	$1.32^{+0.19}_{-0.17}$	$1.27^{+0.15}_{-0.19}$	$1.32^{+0.15}_{-0.24}$	$1.52^{+0.39}_{-0.20}$
2012–03-30	$1.48^{+0.07}_{-0.14}$	$1.34^{+0.14}_{-0.02}$	$1.32^{+0.16}_{-0.16}$	$1.34^{+0.07}_{-0.18}$	$1.32^{+0.16}_{-0.16}$	$1.32^{+0.02}_{-0.16}$	$1.48^{+0.16}_{-0.32}$

Table A.5. Daily $K_0 \times 10^{-4}$ parameter in $AU^2 GV^{-1} s^{-1}$ during FD#058.

Day	3.13 GV	3.46 GV	3.83 GV	4.22 GV	4.65 GV	5.12 GV	5.63 GV
2014–02-23	$1.20^{+0.34}_{-0.16}$	$1.10^{+0.15}_{-0.03}$	$1.18^{+0.02}_{-0.14}$	$1.07^{+0.07}_{-0.15}$	$1.02^{+0.11}_{-0.10}$	$0.87^{+0.18}_{-0.02}$	$0.96^{+0.05}_{-0.16}$
2014–02-24	$1.30^{+0.28}_{-0.22}$	$1.29^{+0.06}_{-0.10}$	$1.30^{+0.07}_{-0.11}$	$1.02^{+0.08}_{-0.05}$	$1.08^{+0.05}_{-0.11}$	$0.97^{+0.06}_{-0.05}$	$0.92^{+0.21}_{-0.01}$
2014–02-25	$1.36^{+0.33}_{-0.17}$	$1.24^{+0.06}_{-0.14}$	$1.36^{+0.11}_{-0.07}$	$1.24^{+0.04}_{-0.11}$	$1.19^{+0.06}_{-0.17}$	$1.02^{+0.08}_{-0.05}$	$1.19^{+0.06}_{-0.27}$
2014–02-26	$1.36^{+0.33}_{-0.11}$	$1.19^{+0.22}_{-0.06}$	$1.47^{+0.07}_{-0.22}$	$1.30^{+0.07}_{-0.01}$	$1.13^{+0.15}_{-0.06}$	$1.10^{+0.03}_{-0.14}$	$1.08^{+0.21}_{-0.06}$
2014–02-27	$1.50^{+0.21}_{-0.21}$	$1.60^{+0.08}_{-0.27}$	$1.44^{+0.03}_{-0.15}$	$1.17^{+0.11}_{-0.06}$	$1.23^{+0.06}_{-0.11}$	$1.12^{+0.05}_{-0.05}$	$1.07^{+0.21}_{-0.05}$
2014–02-28	$1.01^{+0.16}_{-0.16}$	$0.92^{+0.10}_{-0.05}$	$0.92^{+0.02}_{-0.14}$	$0.91^{+0.05}_{-0.11}$	$0.78^{+0.05}_{-0.05}$	$0.76^{+0.05}_{-0.09}$	$0.74^{+0.01}_{-0.11}$
2014–03-01	$1.02^{+0.11}_{-0.11}$	$0.85^{+0.04}_{-0.04}$	$0.85^{+0.04}_{-0.12}$	$0.92^{+0.05}_{-0.05}$	$0.80^{+0.04}_{-0.06}$	$0.80^{+0.04}_{-0.04}$	$0.69^{+0.06}_{-0.03}$
2014–03-02	$0.99^{+0.16}_{-0.24}$	$0.90^{+0.04}_{-0.05}$	$0.78^{+0.11}_{-0.04}$	$0.92^{+0.01}_{-0.07}$	$0.81^{+0.09}_{-0.07}$	$0.74^{+0.07}_{-0.07}$	$0.74^{+0.06}_{-0.09}$
2014–03-03	$0.99^{+0.20}_{-0.14}$	$0.99^{+0.04}_{-0.11}$	$0.92^{+0.14}_{-0.07}$	$0.92^{+0.10}_{-0.01}$	$0.85^{+0.07}_{-0.08}$	$0.78^{+0.14}_{-0.04}$	$0.78^{+0.11}_{-0.05}$
2014–03-04	$1.02^{+0.17}_{-0.11}$	$1.13^{+0.06}_{-0.11}$	$1.02^{+0.06}_{-0.06}$	$0.97^{+0.14}_{-0.05}$	$1.08^{+0.05}_{-0.22}$	$0.91^{+0.06}_{-0.05}$	$0.91^{+0.01}_{-0.11}$
2014–03-05	$1.08^{+0.32}_{-0.15}$	$1.14^{+0.15}_{-0.04}$	$1.14^{+0.10}_{-0.09}$	$1.03^{+0.20}_{-0.05}$	$0.96^{+0.14}_{-0.04}$	$1.13^{+0.06}_{-0.21}$	$0.91^{+0.12}_{-0.04}$
2014–03-06	$1.19^{+0.39}_{-0.11}$	$1.19^{+0.17}_{-0.06}$	$1.24^{+0.06}_{-0.14}$	$1.30^{+0.07}_{-0.11}$	$1.13^{+0.06}_{-0.03}$	$1.13^{+0.11}_{-0.06}$	$0.97^{+0.22}_{-0.05}$
2014–03-07	$1.36^{+0.39}_{-0.17}$	$1.30^{+0.17}_{-0.06}$	$1.30^{+0.06}_{-0.17}$	$1.24^{+0.06}_{-0.17}$	$1.24^{+0.11}_{-0.14}$	$1.13^{+0.11}_{-0.06}$	$1.13^{+0.11}_{-0.11}$
2014–03-08	$1.47^{+0.40}_{-0.19}$	$1.34^{+0.32}_{-0.07}$	$1.47^{+0.02}_{-0.19}$	$1.55^{+0.08}_{-0.26}$	$1.39^{+0.11}_{-0.11}$	$1.34^{+0.07}_{-0.16}$	$1.34^{+0.07}_{-0.21}$
2014–03-09	$1.66^{+0.48}_{-0.27}$	$1.66^{+0.08}_{-0.11}$	$1.66^{+0.16}_{-0.05}$	$1.60^{+0.05}_{-0.13}$	$1.55^{+0.11}_{-0.27}$	$1.23^{+0.32}_{-0.06}$	$1.23^{+0.27}_{-0.06}$
2014–03-10	$1.24^{+0.56}_{-0.50}$	$1.10^{+0.18}_{-0.06}$	$1.08^{+0.11}_{-0.11}$	$1.13^{+0.28}_{-0.11}$	$0.97^{+0.17}_{-0.06}$	$0.97^{+0.06}_{-0.17}$	$0.92^{+0.05}_{-0.18}$
2014–03-11	$1.41^{+0.78}_{-0.28}$	$1.29^{+0.29}_{-0.21}$	$1.08^{+0.45}_{-0.05}$	$1.13^{+0.22}_{-0.03}$	$1.13^{+0.39}_{-0.11}$	$1.10^{+0.18}_{-0.03}$	$0.74^{+0.39}_{-0.04}$
2014–03-12	$1.41^{+0.78}_{-0.49}$	$1.24^{+0.06}_{-0.17}$	$1.47^{+0.16}_{-0.23}$	$0.97^{+0.28}_{-0.05}$	$1.19^{+0.11}_{-0.28}$	$1.30^{+0.07}_{-0.38}$	$0.97^{+0.28}_{-0.06}$
2014–03-13	$1.29^{+0.06}_{-0.18}$	$1.29^{+0.06}_{-0.06}$	$0.92^{+0.18}_{-0.05}$	$0.92^{+0.05}_{-0.05}$	$0.92^{+0.05}_{-0.05}$	$0.74^{+0.18}_{-0.04}$	$0.92^{+0.05}_{-0.05}$
Day	6.19 GV	6.78 GV	7.42 GV	8.12 GV	8.87 GV	9.68 GV	10.6 GV
2014–02-23	$0.80^{+0.13}_{-0.02}$	$0.82^{+0.10}_{-0.20}$	$0.76^{+0.04}_{-0.11}$	$0.66^{+0.14}_{-0.11}$	$0.69^{+0.05}_{-0.16}$	$0.66^{+0.08}_{-0.14}$	$0.71^{+0.22}_{-0.08}$
2014–02-24	$0.97^{+0.05}_{-0.11}$	$0.85^{+0.04}_{-0.06}$	$0.80^{+0.17}_{-0.06}$	$0.74^{+0.18}_{-0.11}$	$0.74^{+0.04}_{-0.19}$	$0.69^{+0.05}_{-0.06}$	$0.92^{+0.10}_{-0.12}$
2014–02-25	$0.97^{+0.06}_{-0.05}$	$0.92^{+0.05}_{-0.12}$	$0.80^{+0.12}_{-0.06}$	$0.74^{+0.12}_{-0.05}$	$0.69^{+0.11}_{-0.11}$	$0.74^{+0.11}_{-0.01}$	$0.85^{+0.11}_{-0.06}$
2014–02-26	$0.92^{+0.05}_{-0.05}$	$0.92^{+0.10}_{-0.07}$	$0.85^{+0.07}_{-0.04}$	$0.97^{+0.06}_{-0.22}$	$0.92^{+0.05}_{-0.18}$	$0.91^{+0.01}_{-0.22}$	$0.92^{+0.16}_{-0.18}$
2014–02-27	$1.01^{+0.11}_{-0.09}$	$1.01^{+0.09}_{-0.09}$	$0.96^{+0.11}_{-0.05}$	$1.01^{+0.05}_{-0.11}$	$0.92^{+0.04}_{-0.07}$	$0.92^{+0.09}_{-0.18}$	$0.91^{+0.21}_{-0.11}$
2014–02-28	$0.71^{+0.04}_{-0.19}$	$0.58^{+0.11}_{-0.05}$	$0.53^{+0.05}_{-0.06}$	$0.51^{+0.05}_{-0.05}$	$0.35^{+0.11}_{-0.02}$	$0.39^{+0.12}_{-0.07}$	$0.44^{+0.16}_{-0.11}$
2014–03-01	$0.63^{+0.03}_{-0.03}$	$0.58^{+0.06}_{-0.02}$	$0.46^{+0.17}_{-0.02}$	$0.58^{+0.03}_{-0.21}$	$0.37^{+0.10}_{-0.02}$	$0.35^{+0.17}_{-0.02}$	$0.58^{+0.06}_{-0.17}$

Table A.5 (*continued*)

Day	3.13 GV	3.46 GV	3.83 GV	4.22 GV	4.65 GV	5.12 GV	5.63 GV
2014–03-02	$0.69^{+0.07}_{-0.06}$	$0.72^{+0.04}_{-0.20}$	$0.53^{+0.11}_{-0.02}$	$0.55^{+0.09}_{-0.09}$	$0.58^{+0.08}_{-0.12}$	$0.49^{+0.14}_{-0.07}$	$0.60^{+0.16}_{-0.11}$
2014–03-03	$0.76^{+0.04}_{-0.12}$	$0.81^{+0.04}_{-0.09}$	$0.74^{+0.06}_{-0.17}$	$0.63^{+0.11}_{-0.08}$	$0.51^{+0.16}_{-0.07}$	$0.63^{+0.13}_{-0.12}$	$0.55^{+0.14}_{-0.13}$
2014–03-04	$0.85^{+0.06}_{-0.04}$	$0.85^{+0.07}_{-0.12}$	$0.80^{+0.11}_{-0.11}$	$0.74^{+0.04}_{-0.11}$	$0.74^{+0.11}_{-0.11}$	$0.74^{+0.06}_{-0.16}$	$0.85^{+0.22}_{-0.06}$
2014–03-05	$1.00^{+0.13}_{-0.14}$	$0.80^{+0.18}_{-0.02}$	$0.82^{+0.20}_{-0.08}$	$0.78^{+0.14}_{-0.22}$	$0.71^{+0.13}_{-0.11}$	$0.74^{+0.11}_{-0.16}$	$0.80^{+0.36}_{-0.09}$
2014–03-06	$1.08^{+0.06}_{-0.17}$	$1.02^{+0.08}_{-0.11}$	$0.80^{+0.22}_{-0.04}$	$0.97^{+0.06}_{-0.17}$	$0.85^{+0.06}_{-0.11}$	$0.80^{+0.17}_{-0.06}$	$0.92^{+0.21}_{-0.07}$
2014–03-07	$1.13^{+0.11}_{-0.06}$	$1.02^{+0.08}_{-0.10}$	$0.97^{+0.11}_{-0.11}$	$0.97^{+0.14}_{-0.11}$	$0.92^{+0.05}_{-0.07}$	$0.92^{+0.05}_{-0.23}$	$1.08^{+0.22}_{-0.17}$
2014–03-08	$1.28^{+0.05}_{-0.21}$	$1.28^{+0.11}_{-0.27}$	$1.12^{+0.16}_{-0.11}$	$1.10^{+0.23}_{-0.14}$	$0.96^{+0.21}_{-0.04}$	$0.96^{+0.16}_{-0.05}$	$1.23^{+0.43}_{-0.11}$
2014–03-09	$1.47^{+0.13}_{-0.24}$	$1.29^{+0.32}_{-0.01}$	$1.28^{+0.05}_{-0.21}$	$1.28^{+0.19}_{-0.18}$	$1.10^{+0.34}_{-0.14}$	$1.34^{+0.32}_{-0.21}$	$1.47^{+0.40}_{-0.24}$
2014–03-10	$0.85^{+0.43}_{-0.06}$	$0.91^{+0.22}_{-0.17}$	$0.69^{+0.23}_{-0.03}$	$0.74^{+0.18}_{-0.17}$	$0.74^{+0.01}_{-0.22}$	$0.74^{+0.23}_{-0.22}$	$0.85^{+0.50}_{-0.17}$
2014–03-11	$0.92^{+0.32}_{-0.12}$	$1.02^{+0.33}_{-0.06}$	$0.92^{+0.21}_{-0.07}$	$1.02^{+0.17}_{-0.28}$	$1.02^{+0.11}_{-0.17}$	$0.63^{+0.22}_{-0.17}$	$1.13^{+0.11}_{-0.39}$
2014–03-12	$0.85^{+0.28}_{-0.12}$	$0.85^{+0.17}_{-0.06}$	$0.74^{+0.37}_{-0.16}$	$0.74^{+0.18}_{-0.18}$	$0.74^{+0.12}_{-0.22}$	$0.69^{+0.22}_{-0.17}$	$0.97^{+0.22}_{-0.33}$
2014–03-13	$0.74^{+0.18}_{-0.04}$	$0.74^{+0.04}_{-0.04}$	$0.74^{+0.04}_{-0.18}$	$0.55^{+0.03}_{-0.03}$	$0.55^{+0.03}_{-0.03}$	$0.55^{+0.37}_{-0.03}$	$0.92^{+0.18}_{-0.37}$

Table A.6. Daily $K_0 \times 10^{-4}$ parameter in $AU^2 GV^{-1} s^{-1}$ during FD#121.

Day	3.13 GV	3.46 GV	3.83 GV	4.22 GV	4.65 GV	5.12 GV	5.63 GV
2017–09-04	$2.14^{+1.86}_{-0.55}$	$2.67^{+0.13}_{-0.71}$	$2.33^{+0.73}_{-0.12}$	$2.51^{+0.73}_{-0.13}$	$3.06^{+1.47}_{-0.73}$	$2.67^{+0.67}_{-0.34}$	$2.70^{+1.47}_{-0.02}$
2017–09-05	$2.01^{+1.97}_{-0.60}$	$2.14^{+0.73}_{-0.14}$	$3.25^{+0.16}_{-0.73}$	$2.51^{+0.37}_{-0.55}$	$2.88^{+0.73}_{-0.55}$	$2.70^{+2.02}_{-0.55}$	$2.70^{+0.55}_{-0.55}$
2017–09-06	$2.67^{+2.00}_{-0.67}$	$2.67^{+0.13}_{-0.13}$	$2.67^{+1.33}_{-0.13}$	$2.67^{+0.13}_{-0.13}$	$2.67^{+0.67}_{-0.13}$	$3.34^{+0.17}_{-0.67}$	$3.34^{+2.66}_{-0.67}$
2017–09-07	$1.80^{+1.77}_{-0.46}$	$2.01^{+0.28}_{-0.21}$	$1.96^{+0.64}_{-0.10}$	$1.96^{+0.05}_{-0.10}$	$2.01^{+0.28}_{-0.37}$	$2.28^{+0.39}_{-0.48}$	$2.12^{+0.32}_{-0.64}$
2017–09-08	$0.59^{+0.15}_{-0.05}$	$0.65^{+0.03}_{-0.03}$	$0.65^{+0.03}_{-0.05}$	$0.65^{+0.03}_{-0.03}$	$0.68^{+0.02}_{-0.03}$	$0.75^{+0.04}_{-0.08}$	$0.75^{+0.04}_{-0.11}$
2017–09-09	$0.74^{+0.28}_{-0.10}$	$0.81^{+0.05}_{-0.11}$	$0.81^{+0.11}_{-0.05}$	$0.81^{+0.05}_{-0.04}$	$0.86^{+0.11}_{-0.04}$	$0.97^{+0.05}_{-0.27}$	$0.97^{+0.14}_{-0.05}$
2017–09-10	$1.16^{+0.18}_{-0.32}$	$1.00^{+0.05}_{-0.05}$	$1.16^{+0.06}_{-0.06}$	$1.16^{+0.18}_{-0.06}$	$1.16^{+0.18}_{-0.06}$	$1.32^{+0.16}_{-0.07}$	$1.16^{+0.18}_{-0.06}$
2017–09-11	$1.48^{+1.12}_{-0.32}$	$1.48^{+0.32}_{-0.14}$	$1.48^{+0.64}_{-0.07}$	$1.64^{+0.16}_{-0.08}$	$1.64^{+0.37}_{-0.08}$	$1.64^{+0.37}_{-0.30}$	$1.48^{+0.48}_{-0.07}$
2017–09-12	$1.52^{+0.97}_{-0.36}$	$1.71^{+0.09}_{-0.40}$	$1.91^{+0.76}_{-0.19}$	$1.81^{+0.29}_{-0.47}$	$1.71^{+0.93}_{-0.10}$	$1.91^{+0.49}_{-0.29}$	$1.81^{+0.29}_{-0.47}$
2017–09-13	$1.32^{+0.48}_{-0.32}$	$1.34^{+0.14}_{-0.18}$	$1.48^{+0.48}_{-0.14}$	$1.32^{+0.32}_{-0.07}$	$1.48^{+0.07}_{-0.16}$	$1.80^{+0.09}_{-0.48}$	$1.80^{+0.09}_{-0.48}$
2017–09-14	$1.34^{+0.67}_{-0.18}$	$1.16^{+0.16}_{-0.06}$	$1.80^{+0.09}_{-0.09}$	$1.48^{+0.32}_{-0.07}$	$1.64^{+0.16}_{-0.30}$	$1.64^{+0.32}_{-0.16}$	$1.64^{+0.32}_{-0.16}$
Day	6.19 GV	6.78 GV	7.42 GV	8.12 GV	8.87 GV	9.68 GV	10.6 GV
2017–09-04	$3.43^{+0.55}_{-1.47}$	$3.34^{+0.67}_{-0.83}$	$2.33^{+1.84}_{-0.37}$	$2.70^{+0.64}_{-0.92}$	$3.43^{+2.57}_{-1.10}$	$2.67^{+1.12}_{-0.67}$	$3.98^{+2.02}_{-1.10}$
2017–09-05	$3.25^{+1.10}_{-0.73}$	$2.67^{+1.12}_{-0.53}$	$2.14^{+1.10}_{-0.37}$	$2.88^{+1.65}_{-0.92}$	$2.70^{+2.02}_{-0.92}$	$2.01^{+1.61}_{-0.05}$	$2.88^{+2.94}_{-0.92}$
2017–09-06	$2.67^{+0.13}_{-0.13}$	$3.34^{+1.33}_{-1.33}$	$4.00^{+0.20}_{-0.67}$	$3.34^{+2.66}_{-0.67}$	$4.00^{+0.67}_{-1.33}$	$3.34^{+1.33}_{-0.67}$	$5.33^{+0.67}_{-2.00}$
2017–09-07	$1.80^{+0.96}_{-0.09}$	$2.01^{+0.10}_{-0.37}$	$2.01^{+0.28}_{-0.21}$	$2.01^{+0.92}_{-0.05}$	$1.80^{+0.48}_{-0.32}$	$2.12^{+0.55}_{-0.48}$	$2.67^{+2.02}_{-0.71}$
2017–09-08	$0.70^{+0.11}_{-0.03}$	$0.75^{+0.04}_{-0.08}$	$0.68^{+0.08}_{-0.08}$	$0.70^{+0.11}_{-0.02}$	$0.75^{+0.04}_{-0.11}$	$0.70^{+0.05}_{-0.05}$	$0.81^{+0.27}_{-0.06}$
2017–09-09	$0.97^{+0.05}_{-0.05}$	$0.93^{+0.15}_{-0.18}$	$0.93^{+0.09}_{-0.07}$	$0.91^{+0.01}_{-0.17}$	$0.91^{+0.21}_{-0.05}$	$0.86^{+0.11}_{-0.12}$	$1.29^{+0.27}_{-0.21}$
2017–09-10	$1.32^{+0.16}_{-0.07}$	$1.16^{+0.16}_{-0.16}$	$1.16^{+0.16}_{-0.06}$	$1.34^{+0.07}_{-0.18}$	$1.16^{+0.18}_{-0.06}$	$1.34^{+0.14}_{-0.02}$	$1.32^{+0.48}_{-0.07}$
2017–09-11	$1.64^{+0.37}_{-0.08}$	$2.01^{+0.10}_{-0.53}$	$1.32^{+0.48}_{-0.07}$	$1.80^{+0.21}_{-0.32}$	$1.64^{+0.37}_{-0.32}$	$2.01^{+0.28}_{-0.37}$	$2.44^{+1.56}_{-0.64}$
2017–09-12	$1.76^{+1.75}_{-0.19}$	$1.80^{+0.60}_{-0.38}$	$2.01^{+0.39}_{-0.44}$	$1.96^{+1.38}_{-0.39}$	$2.12^{+1.74}_{-0.41}$	$1.96^{+1.31}_{-0.48}$	$2.92^{+2.41}_{-0.92}$
2017–09-13	$1.64^{+0.16}_{-0.30}$	$1.48^{+0.48}_{-0.32}$	$1.34^{+0.30}_{-0.07}$	$1.48^{+0.48}_{-0.14}$	$1.34^{+0.14}_{-0.18}$	$1.34^{+0.46}_{-0.18}$	$1.96^{+0.32}_{-0.48}$
2017–09-14	$1.48^{+0.32}_{-0.07}$	$1.64^{+0.16}_{-0.32}$	$1.32^{+0.32}_{-0.07}$	$1.34^{+0.67}_{-0.02}$	$1.64^{+0.16}_{-0.32}$	$1.48^{+0.16}_{-0.16}$	$2.28^{+1.06}_{-0.48}$

References

Adriani, O., Barbarino, G.C., Bazilevskaya, G.A., et al., 2013. Time dependence of the proton flux measured by pamela during the 2006 july-2009 december solar minimum. Astrophys. J. 765, 91. https://doi.org/10.1088/0004-637X/765/2/91.

Aguilar, M., Ali Cavasonza, L., Alpat, B., et al., 2018. Observation of fine time structures in the cosmic proton and helium fluxes with the alpha magnetic spectrometer on the International Space Station. Phys. Rev. Lett. 121 (5), 051101. https://doi.org/10.1103/PhysRevLett.121.051101.

Aguilar, M., Cavasonza, L.A., Ambrosi, G., et al., 2023. Temporal structures in electron spectra and charge sign effects in galactic cosmic rays. Phys. Rev. Lett. 130 (16), 161001. https://doi.org/10.1103/PhysRevLett.130.161001.

Aguilar, M., Cavasonza, L.A., Ambrosi, G., et al., 2021. Periodicities in the Daily Proton Fluxes from 2011 to 2019 Measured by the Alpha Magnetic Spectrometer on the International Space Station from 1 to 100 GV. Phys. Rev. Lett. 127 (27), 271102. https://doi.org/10.1103/PhysRevLett.127.271102.

Aguilar, M., Cavasonza, L.A., Ambrosi, G., et al., 2022. Properties of daily helium fluxes. Phys. Rev. Lett. 128 (23), 231102. https://doi.org/10.1103/PhysRevLett.128.231102.

Arunbabu, K.P., Antia, H.M., Dugad, S.R., et al., 2015. How are forbush decreases related to interplanetary magnetic field enhancements?. Astron. Astrophys. 580, A41. https://doi.org/10.1051/0004-6361/201425115.

Aslam, O.P.M., Bisschoff, D., Ngobeni, M.D., et al., 2021. Time and charge-sign dependence of the heliospheric modulation of cosmic rays. Astrophys. J. 909 (2), 215. https://doi.org/10.3847/1538-4357/abdd35, arXiv:2011.02052.

Balázs, C., van Beekveld, M., Caron, S., et al., 2021. A comparison of optimisation algorithms for high-dimensional particle and astrophysics applications. J. High Energy Phys. 2021 (5), 108. https://doi.org/10.1007/JHEP05(2021)108.

Bartocci, S., Battiston, R., Burger, W.J., et al., 2020. Galactic cosmic-ray hydrogen spectra in the 40–250 MeV Range Measured by the High-energy Particle Detector (HEPD) on board the CSES-01 Satellite between 2018 and 2020. Astrophys. J. 901 (1), 8. https://doi.org/10.3847/1538-4357/abad3e.

Bobik, P., Boella, G., Boschini, M.J., et al., 2012. Systematic investigation of solar modulation of galactic protons for solar cycle 23 using a monte carlo approach with particle drift effects and latitudinal dependence. Astrophys. J. 745, 132. https://doi.org/10.1088/0004-637X/745/2/132.

Bobik, P., Boschini, M.J., Della Torre, S., et al., 2016. On the forward-backward-in-time approach for monte carlo solution of parker's transport equation: One-dimensional case. J. Geophys. Res.: Space Phys. 121 (5), 3920–3930. https://doi.org/10.1002/2015JA022237.

Boschini, M.J., Cavallotto, G., Della Torre, S., et al., 2024. Fast and accurate evaluation of deep-space galactic cosmic ray fluxes with helmod-4/cuda. Adv. Space Res. 74 (9), 4302–4320. https://doi.org/10.1016/j.asr.2024.04.021. Progress in Astrophysics of Cosmic Rays.

Boschini, M.J., Della Torre, S., Gervasi, M., et al., 2022a. A hint of a low-energy excess in cosmic-ray fluorine. Astrophys J 925 (2), 108. https://doi.org/10.3847/1538-4357/ac313d.

Boschini, M.J., Della Torre, S., Gervasi, M., et al., 2022b. Spectra of cosmic-ray sodium and aluminum and unexpected aluminum excess. Astrophys. J. 933 (2), 147. https://doi.org/10.3847/1538-4357/ac7443.

Boschini, M.J., Della Torre, S., Gervasi, M., et al., 2018a. Propagation of cosmic rays in heliosphere: the helmod model. Adv. Space Res. 62 (10), 2859–2879. https://doi.org/10.1016/j.asr.2017.04.017.

Boschini, M.J., Della Torre, S., Gervasi, M., et al., 2019. The helmod model in the works for inner and outer heliosphere: From ams to voyager probes observations. Adv. Space Res. 64 (12), 2459–2476. https://doi.org/10.1016/j.asr.2019.04.007.

Boschini, M.J., Della Torre, S., Gervasi, M., et al., 2022c. The transport of galactic cosmic rays in heliosphere: The HELMOD model compared with other commonly employed solar modulation models. Adv. Space Res. 70 (9), 2636–2648. https://doi.org/10.1016/j.asr.2022.03.026.

Boschini, M.J., Della Torre, S., Gervasi, M., et al., 2017. Solution of heliospheric propagation: unveiling the local interstellar spectra of cosmic-ray species. Astrophys. J. 840, 115. https://doi.org/10.3847/1538-4357/aa6e4f.

Boschini, M.J., Della Torre, S., Gervasi, M., et al., 2018b. Deciphering the local interstellar spectra of primary cosmic-ray species with helmod. Astrophys. J. 858 (1), 61. https://doi.org/10.3847/1538-4357/aabc54.

Boschini, M.J., Della Torre, S., Gervasi, M., et al., 2018c. Helmod in the works: from direct observations to the local interstellar spectrum of cosmic-ray electrons. Astrophys. J. 854 (2), 94. https://doi.org/10.3847/1538-4357/aaa75e.

Boschini, M.J., Della Torre, S., Gervasi, M., et al., 2020a. Deciphering the local interstellar spectra of secondary nuclei with the galprop/helmod framework and a hint for primary lithium in cosmic rays. Astrophys. J. 889 (2), 167. https://doi.org/10.3847/1538-4357/ab64f1.

Boschini, M.J., Della Torre, S., Gervasi, M., et al., 2020b. Inference of the local interstellar spectra of cosmic-ray nuclei $z < 28$ with the GalProp-HelMod framework. Astrophys. J. Supplement 250 (2), 27. https://doi.org/10.3847/1538-4365/aba901.

Boschini, M.J., Della Torre, S., Gervasi, M., et al., 2021. The discovery of a low-energy excess in cosmic-ray iron: Evidence of the past supernova activity in the local bubble. Astrophys J 913 (1), 5. https://doi.org/10.3847/1538-4357/abf11c.

Burger, R.A., Hattingh, M., 1998. Toward a realistic diffusion tensor for galactic cosmic rays. Astrophys. J. 505, 244–251. https://doi.org/10.1086/306152.

Caballero-Lopez, R.A., Moraal, H., 2004. Limitations of the force field equation to describe cosmic ray modulation. J. Geophys. Res.-Space 109 (A18), 1101. https://doi.org/10.1029/2003JA010098.

Cane, H., 2000. Coronal mass ejections and forbush decreases. Spac. Sc. Rev. 93, 55–77. https://doi.org/10.1023/A:1026532125747.

Cane, H.V., Richardson, I.G., 2003. Interplanetary coronal mass ejections in the near-earth solar wind during 1996–2002. J. Geophys. Res.: Space Phys. 108 (A4). https://doi.org/10.1029/2002JA009817.

Cavallotto, G., Della Torre, S., La Vacca, G., et al., 2025. Cosmica: a novel parallel gpu code for cosmic rays propagation in heliosphere. In: to be published on IEEE Conference proceedings.

Della Torre, S., Bobik, P., Boschini, M.J., et al., 2012. Effects of solar modulation on the cosmic ray positron fraction. Adv. Space Res. 49, 1587–1592. https://doi.org/10.1016/j.asr.2012.02.017.

Dunzlaff, P., Strauss, R.D., Potgieter, M.S., 2015. Solving Parker's transport equation with stochastic differential equations on GPUs. Comput. Phys. Commun. 192, 156–165. https://doi.org/10.1016/j.cpc.2015.03.008.

Effenberger, F., Fichtner, H., Scherer, K., et al., 2012. Anisotropic diffusion of Galactic cosmic ray protons and their steady-state azimuthal distribution. Astron. Astrophys. 547, A120. https://doi.org/10.1051/0004-6361/201220203.

Engelbrecht, N.E., Effenberger, F., Florinski, V., et al., 2022. Theory of Cosmic Ray Transport in the Heliosphere. Spac. Sc. Rev. 218 (4), 33. https://doi.org/10.1007/s11214-022-00896-1.

Engelbrecht, N.E., Vogt, A., Herbst, K., et al., 2022. Revisiting the revisited palmer consensus: New insights from jovian electron transport. Astrophys J 929 (1), 8. https://doi.org/10.3847/1538-4357/ac58f5.

Falkner, S., Klein, A., & Hutter, F. (2018). Bohb: Robust and efficient hyperparameter optimization at scale. URL: https://arxiv.org/abs/1807.01774. arXiv:1807.01774.

Fisk, L., 1971. Solar modulation of galactic cosmic rays. J. Geophys. Res.-Space 76 (1), 221–226. https://doi.org/10.1029/JA076i001p00221.

Forbush, S.E., 1937. On the effects in cosmic-ray intensity observed during the recent magnetic storm. Phys. Rev. 51, 1108–1109. https://doi.org/10.1103/PhysRev.51.1108.3.

Forbush, S.E. (1954). World-wide cosmic ray variations, 1937–1952. Journal of Geophysical Research (1896–1977), 59(4), 525–542. doi:10.1029/JZ059i004p00525.

Gleeson, L.J., Axford, W.I., 1967. Cosmic rays in the interplanetary medium. Astrophys. J. 149, L115–L118. https://doi.org/10.1086/180070.

Gleeson, L.J., Axford, W.I., 1968. The Compton-Getting Effect. Astrophys. Space Sci. 2, 431–437. https://doi.org/10.1007/BF02175919.

Gleeson, L.J., Urch, I.H., 1971. Energy losses and modulation of galactic cosmic rays. Astrophys. Space Sci. 11, 288–308. https://doi.org/10.1007/BF00661360.

Iucci, N., Parisi, M., Storini, M., et al., 1979. Forbush decreases: Origin and development in the interplanetary space. Il Nuovo Cimento C 2 (1), 52. https://doi.org/10.1007/BF02507712.

Jokipii, J.R., 1966. Cosmic-Ray Propagation. I. Charged Particles in a Random Magnetic Field. Astrophys. J. 146, 480. https://doi.org/10.1086/148912.

Jokipii, J.R., 1971. Propagation of cosmic rays in the solar wind. Rev. Geoph. Space Phys. 9, 27–87. https://doi.org/10.1029/RG009i001p00027.

Jokipii, J.R., Kota, J., 1989. The polar heliospheric magnetic field. Geoph. Res. Lett. 16 (1), 1–4. https://doi.org/10.1029/GL016i001p00001.

Jokipii, J.R., Levy, E.H., 1977. Effects of particle drifts on the solar modulation of galactic cosmic rays. Astrophys. J. Lett. 213, L85–L88. https://doi.org/10.1086/182415.

Jokipii, J.R., Levy, E.H., Hubbard, W.B., 1977. Effects of particle drift on cosmic-ray transport. I - General properties, application to solar modulation. Astrophys. J. 213, 861–868. https://doi.org/10.1086/155218.

Jokipii, J.R., Parker, E.N., 1970. on the Convection, Diffusion, and Adiabatic Deceleration of Cosmic Rays in the Solar Wind. Astroph. J. 160, 735–744. https://doi.org/10.1086/150465.

Jokipii, J.R., Thomas, B., 1981. Effects of drift on the transport of cosmic rays. IV - Modulation by a wavy interplanetary current sheet. Astrophys. J. 243, 1115–1122. https://doi.org/10.1086/158675.

Kopp, A., Büsching, I., Strauss, R.D., et al., 2012. A stochastic differential equation code for multidimensional Fokker-Planck type problems. Comput. Phys. Commun. 183, 530–542. https://doi.org/10.1016/j.cpc.2011.11.014.

Kühl, P., Dresing, N., Heber, B., et al., 2017. Solar Energetic Particle Events with Protons Above 500 MeV Between 1995 and 2015 Measured with SOHO/EPHIN. Sol. Phys. 292 (1), 10. https://doi.org/10.1007/s11207-016-1033-8.

Leclercq, F., 2018. Bayesian optimization for likelihood-free cosmological inference. Physical Review D 98 (6). https://doi.org/10.1103/physrevd.98.063511.

Liu, W., Guo, J., Wang, Y., et al., 2024. A comprehensive comparison of various galactic cosmic-ray models to the state-of-the-art particle and radiation measurements. Astrophys. J. Suppl. Ser. 271 (1), 18. https://doi.org/10.3847/1538-4365/ad18ad.

Lockwood, J.A., Webber, W.R., Debrunner, H., 1991. Forbush decreases and interplanetary magnetic field disturbances: Association with magnetic clouds. Journal of Geophysical Research: Space Physics 96 (A7), 11587–11604. https://doi.org/10.1029/91JA01012.

Luo, X., Potgieter, M.S., Zhang, M., et al., 2017. A numerical study of forbush decreases with a 3d cosmic-ray modulation model based on an sde approach. Astrophys J 839 (1), 53. https://doi.org/10.3847/1538-4357/aa6974.

Luo, X., Potgieter, M.S., Zhang, M., et al., 2018. A study of electron forbush decreases with a 3d sde numerical model. Astrophys J 860 (2), 160. https://doi.org/10.3847/1538-4357/aac5f2.

Mahendran, N., Wang, Z., Hamze, F. et al. (2012). Adaptive mcmc with bayesian optimization. In N.D. Lawrence, & M. Girolami (Eds.), Proceedings of the Fifteenth International Conference on Artificial Intelligence and Statistics (pp. 751–760). La Palma, Canary Islands: PMLR volume 22 of Proceedings of Machine Learning Research. URL: https://proceedings.mlr.press/v22/mahendran12.html.

Matthaeus, W.H., Qin, G., Bieber, J.W., et al., 2003. Nonlinear Collisionless Perpendicular Diffusion of Charged Particles. Astrophys. J. Letter 590, L53–L56. https://doi.org/10.1086/376613.

Moloto, K.D., Engelbrecht, N.E., Strauss, R.D., et al., 2019. Numerical integration of stochastic differential equations: A parallel cosmic ray modulation implementation on Africa's fastest computer. Adv. Space Res. 63 (1), 626–639. https://doi.org/10.1016/j.asr.2018.08.048.

Palmer, I.D., 1982. Transport coefficients of low-energy cosmic rays in interplanetary space. Rev. Geophys. Space Ge. 20, 335–351. https://doi.org/10.1029/RG020i002p00335.

Parker, E.N., 1965. The passage of energetic charged particles through interplanetary space. Plan. Space Sci. 13, 9–49. https://doi.org/10.1016/0032-0633(65)90131-5.

Potgieter, M., Ferreira, S., 2001. Modulation of cosmic rays in the heliosphere over 11 and 22 year cycles: a modelling perspective. Adv. Space Res. 27 (3), 481–492. https://doi.org/10.1016/S0273-1177(01)00080-1.

Potgieter, M.S., 2013. Solar Modulation of Cosmic Rays. Living Rev. Sol. Phys. 10 (1), 3. https://doi.org/10.12942/lrsp-2013-3, arXiv:1306.4421.

Potgieter, M.S., Moraal, H., 1985. A drift model for the modulation of galactic cosmic rays. Astrophys. J. 294 (part 1), 425–440. https://doi.org/10.1086/163309.

Qin, G., Zhang, L.-H., 2014. The modification of the nonlinear guiding center theory. Astrophys J 787 (1), 12. https://doi.org/10.1088/0004-637X/787/1/12.

Rankin, J., Bindi, V., Bykov, A. et al. (2022a). Galactic cosmic rays throughout the heliosphere and in the very local interstellar medium. Space Science Reviews, 218(5), Article number: 42. doi:10.1007/s11214-022-00912-4.

Rankin, J.S., McComas, D.J., Leske, R.A. et al. (2022b). Anomalous Cosmic-Ray Oxygen Observations into 0.1 au. Astrophys. J., 925(1), 9. doi:10.3847/1538-4357/ac348f.

Roussel, R., Edelen, A.L., Boltz, T., et al., 2024. Bayesian optimization algorithms for accelerator physics. Phys. Rev. Accel. Beams 27, 084801. https://doi.org/10.1103/PhysRevAccelBeams.27.084801.

Ruffolo, D., Pianpanit, T., Matthaeus, W.H., et al., 2012. Random ballistic interpretation of nonlinear guiding center theory. Astrophys. J. Lett. 747 (2), L34. https://doi.org/10.1088/2041-8205/747/2/L34.

Santoni, M.L., Raponi, E., Leone, R.D., et al., 2024. Comparison of high-dimensional bayesian optimization algorithms on bbob. ACM Trans. Evol. Learn. Optim. 4 (3). https://doi.org/10.1145/3670683.

Shahriari, B., Swersky, K., Wang, Z., et al., 2016. Taking the human out of the loop: A review of bayesian optimization. Proc. IEEE 104 (1), 148–175. https://doi.org/10.1109/JPROC.2015.2494218.

Shalchi, A., 2010. A unified particle diffusion theory for cross-field scattering: Subdiffusion, recovery of diffusion, and diffusion in three-dimensional turbulence. Astrophys. J. Lett. 720 (2), L127. https://doi.org/10.1088/2041-8205/720/2/L127.

Shalchi, A., Schlickeiser, R., 2004. The parallel mean free path of heliospheric cosmic rays in composite slab/two-dimensional geometry. I. The damping model of dynamical turbulence. Astrophys. J. 604, 861–873. https://doi.org/10.1086/382065.

Simpson, J.A., Anglin, J.D., Balogh, A., et al., 1992. The ULYSSES Cosmic Ray and Solar Particle Investigation. Astronomy and Astrophysics Supplement Series 92, 365–399.

Solanik, M., Bobik, P., & Genci, J. (2021). Cosmic rays modulation in heliosphere models on GPU. In Proceedings of 37th International Cosmic Ray Conference — PoS(ICRC2021) (p. 1320). volume 395. doi:10.22323/1.395.1320.

Solanik, M., Bobik, P., Genci, J., 2023. Geliosphere - parallel cpu and gpu based models of cosmic ray modulation in the heliosphere. Comput. Phys. Commun. 291, 108847. https://doi.org/10.1016/j.cpc.2023.108847.

Stone, E.C., Vogt, R.E., McDonald, F.B., et al., 1977. Cosmic ray investigation for the Voyager missions; energetic particle studies in the outer heliosphere—And beyond. Spac. Sc. Rev. 21 (3), 355–376. https://doi.org/10.1007/BF00211546.

Strauss, R., Potgieter, M., Ferreira, S., 2013. Modelling and observing jovian electron propagation times in the inner heliosphere. Adv. Space Res. 51 (3), 339–349. https://doi.org/10.1016/j.asr.2012.09.035.

Tomassetti, N., Bertucci, B., Fiandrini, E. et al. (2025). Propagation times and energy losses of cosmic protons and antiprotons in interplanetary space. Galaxies, 13(2). URL: https://www.mdpi.com/2075-4434/13/2/23. doi:10.3390/galaxies13020023.

Tomassetti, N., Orcinha, M., Barão, F., et al., 2017. Evidence for a time lag in solar modulation of galactic cosmic rays. The Astrophysical Journal Letters 849 (2), L32. https://doi.org/10.3847/2041-8213/aa9373.

Vogt, A., Engelbrecht, N.E., Strauss, R.D., et al., 2020. The residence-time of jovian electrons in the inner heliosphere. Astron. Astrophys. 642, A170. https://doi.org/10.1051/0004-6361/201936897.

Vogt, A., Engelbrecht, N.E., Strauss, R.D., et al., 2020. The residence-time of Jovian electrons in the inner heliosphere. Astron. Astrophys. 642, A170. https://doi.org/10.1051/0004-6361/201936897.

Vos, E.E., Potgieter, M.S., 2016. Global Gradients for Cosmic-Ray Protons in the Heliosphere During the Solar Minimum of Cycle 23/24. Sol. Phys. 291 (7), 2181–2195. https://doi.org/10.1007/s11207-016-0945-7, arXiv:1608.01688.

Wang, S., Bindi, V., Consolandi, C., et al., 2023. Properties of forbush decreases with ams-02 daily proton flux data. Astrophys J 950 (1), 23. https://doi.org/10.3847/1538-4357/acca1b.

Wawrzynczak, A., Alania, M., 2008. Modeling of the recurrent forbush effect of the galactic cosmic ray intensity and comparison with the experimental data. Adv. Space Res. 41 (2), 325–334. https://doi.org/10.1016/j.asr.2007.05.017.

Wawrzynczak, A., Alania, M.V., 2010. Modeling and data analysis of a forbush decrease. Adv. Space Res. 45 (5), 622–631. https://doi.org/10.1016/j.asr.2009.09.005.

Yang, Y., Luo, X., Song, X. et al. (2025). A numerical study of unusual flux decreases for cosmic ray protons and electrons observed by ams in 2017. Astron. Astrophys., Forthcoming article, doi:10.1051/0004-6361/202452416.

Yu, X., Lu, H., Le, G., et al., 2010. Influence of magnetic clouds on variations of cosmic rays in november 2004. Sol Phys 263, 223–237. https://doi.org/10.1007/s11207-010-9522-7.

Zhao, L.L., Qin, G., Zhang, M., et al., 2014. Modulation of galactic cosmic rays during the unusual solar minimum between cycles 23 and 24. J. Geophys. Res. (Space Phys.) 119 (3), 1493–1506. https://doi.org/10.1002/2013JA019550.